Dendritically-Drained Peat Plateaus: A Distinctive Thaw-Sensitive Organic-Rich Permafrost Landsystem in Northwestern Canada

Authors: Chiasson, A[1,2,3]., La Farge-England, C.[4], Van der Sluijs, J[5]., Rudy, A.C.A[3]., Kokelj, S.V[3] & Froese, D.G[1,2]

1. Department of Earth and Atmospheric Sciences, University of Alberta, Edmonton, Canada.
2. Permafrost Archives Science Laboratory, Department of Earth and Atmospheric Sciences, University of Alberta, Edmonton, Canada.
3. NWT Geological Survey, Government of Northwest Territories, Yellowknife, Canada.
4. Department of Biological Sciences, University of Alberta, Edmonton, Alberta T6G 2E9, Canada.
5. NWT Centre for Geomatics, Government of Northwest Territories, Yellowknife, Canada

This is a non-peer preprint submitted to EarthArXiv of a manuscript submitted for peer-review to the Journal Permafrost and Periglacial Processes.

Correspondence: Alexandre Chiasson, Ph.D. candidate at Department of Earth and Atmospheric Science, University of Alberta (Alberta).

CONTACT INFORMATION:
Email: Alexandre_Chiasson@gov.nt.ca, duane.froese@ualberta.ca

Duane Froese: https://orcid.org/0000-0003-1032-5944
Alexandre Chiasson: https://orcid.org/0000-0003-1852-0138
Jurjen Van der Sluijs: https://orcid.org/0000-0002-9244-1756
Ashley Rudy: https://orcid.org/0000-0002-7977-5719
Steve Kokelj: https://orcid.org/0000-0002-2840-2605
Catherine La Farge-England: https://orcid.org/0000-0001-6293-021X

Funding Information: Fonds de recherche du Québec – Nature et technologies and Northern Science Training Program from Polar Knowledge Canada, Weston Foundation in Northern Research, and GIS ERSI Award to AC; NSERC Discovery Grant and Northern Research Supplement and support from NWT Geological Survey, PermafrostNet and Polar Continental Shelf (to DF).

KEYWORDS: Permafrost, Channelized fen, Peat plateau, Taiga Plain, Dendritic drainage pattern, Permafrost landsystem

The authors declare there are no conflicts of interest for this manuscript.

Abstract

Peatlands in northwestern Canada comprise one of the most thaw-sensitive and carbon-rich permafrost landscapes of North America, and undergo rapid thaw due to surface disturbance and climate change. Dendritically-drained peat plateaus (DPPs) are a distinctive permafrost landform assemblage characterized by branching networks of channelized fens and bogs dissecting raised peat plateaus with relatively thin, carbon-rich permafrost underlain by ice-rich till. Using remote sensing, field observations, and geophysical methods, we describe the morphology, permafrost conditions, and developmental history of DPPs and mapped their distribution across the Northwest Territories. These landform assemblages cover ~22,500 km² of the Taiga Plains, forming in the early Holocene (~10,000 cal yr BP) on gently sloping till plains above glacial Lake Mackenzie. In the central Mackenzie Valley, DPPs consist of ~2 m of peat over ice-rich diamict with abundant ground ice. Electrical resistivity tomography surveys indicate that permafrost is typically less than 20 m thick beneath peat plateaus. Taliks underlie channelized fens, promoting advection and lateral heat transfer, which account for thin permafrost and rapid lateral erosion along plateau margins. Variation in assemblages along a latitudinal climate gradient gives rise to contrasting morphologies: southern regions feature larger basins, collapse scars, and wide channelized fens, while northern landscapes have higher densities of narrower fens, smaller collapse scars, and more extensive permafrost plateaus. The long-term interaction between ground ice, geological history, ecology and regional climate drives the development of diverse surface features, allowing us to conceptually define these landform assemblages as a regional permafrost landsystem.

1. Introduction

Peatlands in the Taiga Plains ecozone of northwestern Canada represent one of the most carbon-rich and thaw-sensitive permafrost regions in the world [1,2]. Significant warming over recent decades [3,4] amplified by increasing wildfires, has driven top-down permafrost thaw and landscape change in permafrost peatlands in the Taiga Plains [2,5]. Research has also focused on permafrost-hydrology interactions [6-8], showing that the degradation of permafrost plateau improves the connectivity of collapse scars and fens5-9, decreasing water storage and increasing downstream discharge [10-12]. The linkages between hydrology and permafrost create a positive feedback that accelerates permafrost thaw [11,13], as well as increasing concentrations of dissolved organic carbon (DOC) [14] and methylmercury [15]. Zoltai and Tarnocai [16] describe organic terrains across this region as being dominated by frozen peat plateaus and palsas with few collapse scars, and some peatlands are associated with unfrozen fens. However, little is known about the variability in morphology, permafrost configuration, and thaw sensitivity of organic-rich landscapes across much of this region [17].

Peat plateaus characterized by dendritic drainage patterns represent a distinctive and understudied permafrost peatland landform assemblage prevalent in northwestern Canada. Dendritic drainage networks have been widely described in the context of erosional gully systems and carbon flux in degraded blanket peatlands [18-20], however, these studies address non-permafrost environments where dendritic patterns arise from erosional dissection. The branching drainage patterns described here are linked to permafrost dynamics, reflecting the natural geometry of channelized fen networks, collapse scars, and thermokarst basins that develop through differential thaw of ice-rich peat plateau. These landform assemblages are hereafter referred to as dendritically-drained peat plateaus (DPPs). We explore the linkages between landscape genesis, climate history, and ecology [21-22] to develop conceptual representation of the formation of dendritically-drained peat plateau landform assemblages. Through applying a permafrost landsystem framework, the terrain is viewed as a product of interconnected biophysical elements that manifest as landform assemblages indicating characteristic substrate, ground ice, ground thermal, and vegetation conditions [23]. Conceptualizing DPPs as distinctive, organic-rich, thaw-sensitive landform assemblages within a

permafrost landsystem framework enables their formation, permafrost characteristics, and potential trajectories under climate change to be explained.

In this study, we investigate the genesis, distribution, and characteristics of DPPs to understand how these thaw-sensitive, organic-rich permafrost landform assemblages vary with terrain and climate conditions. Specifically, we 1) describe the morphology, soil, and permafrost properties and configuration of DPPs; 2) investigate their spatial distribution with respect to glacial history and deposit type; and 3) explore their morphological variation across the ecoclimate gradient of the study area (Taiga Plain ecozone). We used remote sensing imagery to map these assemblages, coupled with field observations and geophysical surveys at sites in the Central Mackenzie valley, to describe their morphological, organic carbon, and permafrost characteristics. We applied permafrost landsystems concepts to explain their genesis and how hydrological, ecosystem, and climate interact in their development, variation in morphology, and thaw sensitivity.

2. Background and Regional Setting

2.1. Defining Dendritically-drained peat plateau

In this study, we define a DPP as a permafrost peatland landform assemblage that exhibits a branching network of channelized fens that dissect the permafrost peat plateau and connect other similarly oriented channel fens, collapse scars, and shallow basins (**Figure 1; Figure S1 in Supporting Information S1**). Local vegetation is dominated by open-canopied black spruce (*Picea mariana*) forests with a ground cover of light-colored reindeer lichens (*Cladina stellaris* and *Cladina stygia*) on peat plateaus, contrasting with dark brown mosses in channelized fens and collapse scars. Reindeer lichens grow naturally on all dendritic peat plateaus, making the identification of DPPs relatively straightforward in undisturbed areas (**Figure 1**). However, these ecosystems are highly susceptible to wildfire disturbances, which can destroy the lichen cover and accelerate permafrost thaw, thereby making the identification of DPPs more challenging in post-fire landscapes (**Figure 1c,e**).

Dendriticically-drained refers to hydrological drainage networks with branching tributaries that typically form on or into gentle regional slopes [24-25], and best describe drainage patterns of these assemblages. Similar features defined by Glaser [26] as streamlined bog islands in the Great Slave and Great Bear Lake lowlands, which are water tracks fed by minerotrophic seeps associated with collapse scars. However, the landforms are identified in both permafrost and non-permafrost environments. Vitt et al. [17] defined "peat plateaus with collapse scars" as isolated, circular, or interconnected forested peat plateaus with drainage channels, surrounded by fens. Zoltai [27] and Quinton et al. [6] described "channel fens" as wide, dendritic-like patterns oriented parallel to topographic slopes that transport water laterally to basin outlets. Based on their repeated and distinct drainage patterns, we identify these permafrost peatland landform assemblages as DPPs, or simply termed dendritic peat plateaus.

2.2. Study area: the Taiga Plains ecozone

The Taiga Plains ecozone (550,000 km^2) is a low-relief, organic-rich region centred on the Mackenzie River valley (**Figure 1**). It contains Canada's second largest peatland complex, after the Hudson Bay Lowlands, characterized by thick organic deposits and poorly drained terrain [1]. The ecozone follows a latitudinal gradient, transitioning from southern boreal forest to northern subarctic forest-tundra. Vegetation is primarily dominated by *Picea mariana* (black spruce) and *Larix laricina* (larch) in poorly drained areas, while well-drained sites host *Picea glauca* (white spruce) and deciduous species like *Populus tremuloides* (aspen) [28]. Permafrost and peatland morphology vary significantly along this gradient. The northern continuous permafrost zone is dominated by polygonal peat plateaus. Conversely, the southern discontinuous permafrost zone features complex mosaics of peat plateaus, palsas, unfrozen fens and patterned fens, and collapse scars are more extensive with fires having a major influence on peatland degradation and development [26,29].

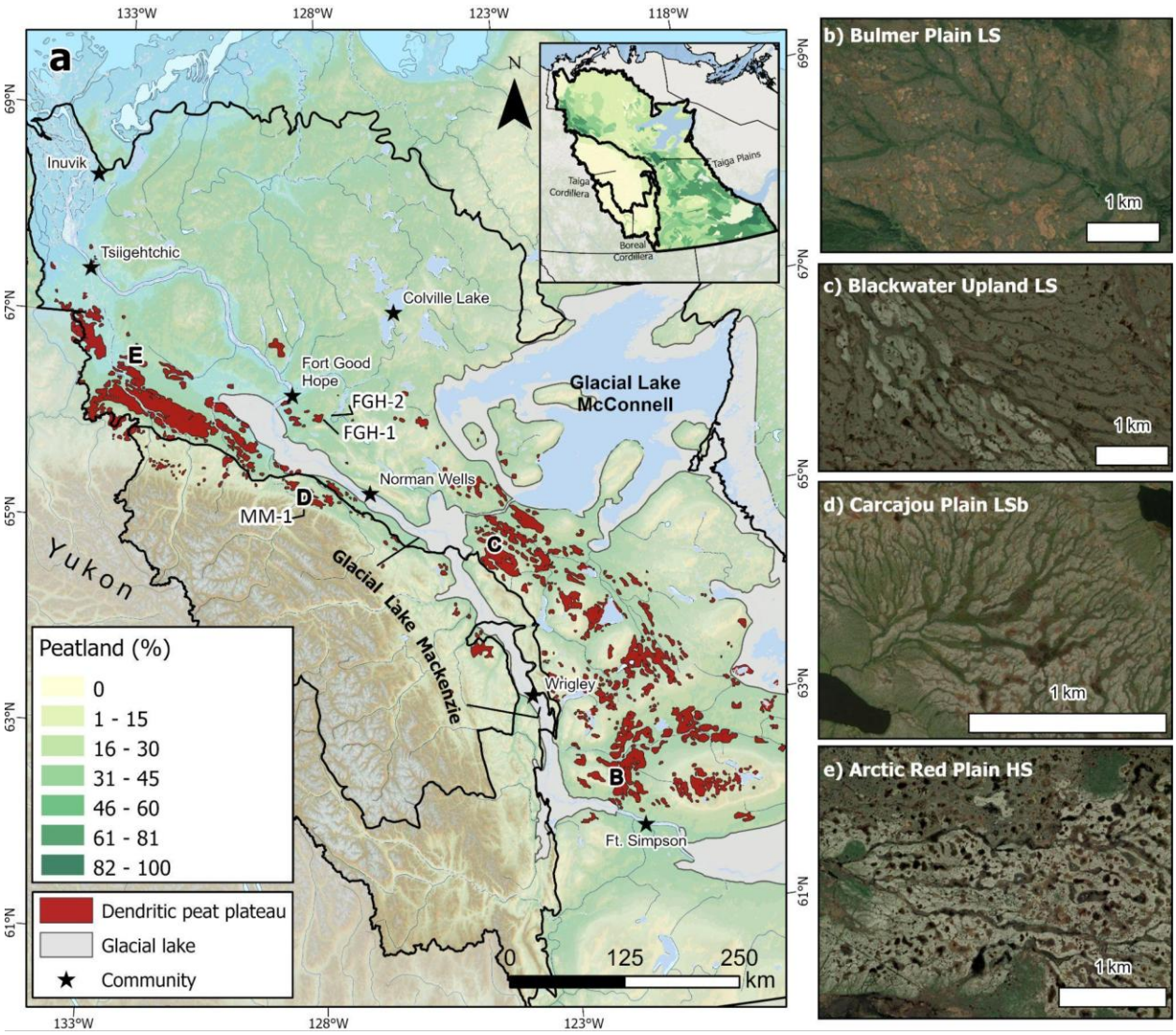

Figure 1. a) Distribution of DPPs (red) across the Taiga Plains ecozone. Maximum extent of glacial Lakes Mackenzie and McConnell from Smith [31,32] and Couch and Eyles [34]. Peatland (%) layer modified from Tarnocai et al. [1]. Baselayer sources from GeoGratis. Letters (b to e) refer to DPP example locations. b) DPPs in extensive discontinuous permafrost showing large areas of collapse scars and basins connected by well-defined dendritic drainage patterns, Bulmer Plain LS Level IV ecoregion north of Fort Simpson (62.4294, -121.8219). c) Burned (1998) DPPs located in the Blackwater Upland LS Level IV ecoregion south of Tulít'a (64.6206, -124.0567). d) DPP with extensive dendritic fen networks in extensive discontinuous permafrost near the Mackenzie Mountains, Carcajou Plain LSb Level IV ecoregion (65.2288, -128.2927). e) DPPs in continuous permafrost with narrow channelized fens and collapse bogs and basins in the Arctic Red Plain HS near Tsiigehtchic (66.6063, -132.6288). High-resolution base imagery retrieved from the ESRI World Imagery layer (accessed February 2026).

2.3. Central Mackenzie Valley – Studied DPPs

Three DPP sites were selected for site-level investigation in the central Mackenzie Valley within the Taiga Plains ecoregion: MM-01 (**Figure 1**), and FGH-1 and FGH-2 (**Figure 1**). This region is defined by undulating topography that gradually descends from the Mackenzie Mountains to the west toward the Mackenzie River, and rises east-northeast toward local mountains such as the Norman Range and McConnell ranges. The area was shaped by continental glaciation and deglaciation, and then by subsequent post-glacial lakes Mackenzie and McConnell [30-33]. The maximum extent of the Laurentide Ice Sheet glaciation occurred after ca. 18 ka yr BP and the central Mackenzie Valley became ice-free by ca. 14 ka yr BP [33]. The formation of glacial Lake Mackenzie in the region was due to isostatic uplift forming a barrier near the Ramparts of the Mackenzie River, near Fort Good Hope [30-32]. At its maximum, glacial Lake Mackenzie extended ~800 km between Fort Simpson to the Ramparts near Fort Good Hope [30,31,34] (**Figure 1**). Extensive deposits of glaciolacustrine sediments from glacial Lake Mackenzie occupy the lowland landscape along the Mackenzie River to an elevation of ca. 150 m a.s.l. [31]. The surficial geology includes tills deposits across rolling plains, drumlinoid ridges and megascale lineations oriented S-N [35], areas of hummocky terrain, and glaciofluvial deposits inherited from late Wisconsinan deglaciation [33, 36]; Holocene deposits, including alluvial and lacustrine sediments, are present along the Mackenzie River [36]. Peatlands are mainly present in the western part of the Central Mackenzie valley and extend to the southern portion of the Taiga Plains [1,2,37].

The region has a subarctic climate characterized by long, cold winters and short, hot summers. In Norman Wells, the mean annual air temperature from 1945 to 2021 is –5.46°C. The region experiences an average annual rainfall of ~183 mm and an average snowfall of ~150 cm. In Norman Wells, the mean annual air temperature (MAAT) for the 1991–2020 period is −4.8 °C. Air temperatures have increased at a rate of about 0.70°C/decade since 1990, with 5 of the warmest years occurring since 2015 [38]. Permafrost follows a latitudinal gradient transitioning from continuous in the north to discontinuous and sporadic in the south. Near Fort Simpson, permafrost is thin (1.5–17 m) and associated with peatlands featuring dry ground surfaces, including peat plateaus and palsas, with permafrost covering 10–50% of the area [39,40]. Between Wrigley and Fort Good Hope, permafrost occupies 50–90% of the landscape. Thickness varies with drainage conditions, with well-drained mineral soils hosting thicker permafrost

exceeding 20 m, while poorly drained, organic-rich areas such as peatlands have thinner permafrost under 10 m due to interactions between surface water and organic deposits [41,42]. Permafrost in this region is relatively warm (–2°C to –0.2°C) and near thawing, having warmed by about 0.1°C per decade since 1984 [3].

3. Methods

3.1. Regional scale analysis

We implemented a grid-cell inventory to evaluate the morphology and distribution of DPPs across the Taiga Plains Ecozone using 2018 SPOT 6/7 (1.5 m) 2018 true-color and false-color satellite imagery. The area of interest was divided into grid cells measuring 1.25 x 1.25 km nested within the 7.5 x 7.5 km Thermokarst Mapping Collective (TMC) grids [43], and the presence or absence of DPPs within each grid cell was recorded in an ESRI ArcGIS Pro 3.0.1 geodatabase. We also compared our fine-scale DPPs distribution with the TMC datasets using a spatial overlap analysis to quantify agreement between the two mapping products.

To explore regional variability in DPP morphology and drainage assemblages, we delineated individual DPP assemblages from 1.25 × 1.25 km grid cells using high-resolution 2 m-ArcticDEM [44] through watershed delineation, as channelized fens define natural drainage boundaries. For each assemblage, we randomly selected DPPs within each ecoregion of the Taiga Plains to calculate morphometric indices including (1) basin area, (2) elongation ratio (Re) (basin width/length), (3) compactness coefficient (Cc) (basin perimeter/circle perimeter), (4) basin relief (elevation range), and (5) mean slope [45,46]. Within randomly selected DPPs, we manually digitized 6) collapse scars using high-resolution ESRI ArcGIS Pro basemap imagery and measured 7) channelized fen widths by placing points at opposing fen edges and calculating perpendicular distances. We classified collapse scars and channelized fen coverage as low (0–25%), medium (25–50%), or high (75–100%). Using ArcticDEM, we estimated the average slope and elevation for each 1.25 x 1.25 km grid cell containing a DPP. Non-parametric statistical tests were employed due to non-normal distributions and heterogeneous variances (Shapiro-Wilk and Levene's tests, $p < 0.001$), including Kruskal-Wallis tests for ecoregion comparisons, Mann-Whitney U tests for elongated versus intermediate basins, Chi-square tests (χ^2) for difference in basin shape

distribution between ecoregions, and Spearman's rank correlations for variable relationships. All statistical analyses used $\alpha = 0.05$. All statistical analyses and figures were conducted and created using RStudio (version 2025.09.0) or ArcPy in Esri ArcGIS Pro. Coding assistance for R and ArcPy development and troubleshooting was provided by ClaudeAI.

The Daymet air temperature dataset (1 x 1 km^2) [47] was used to retrieve annual temperature and precipitation (snow and rainfall combined) data from 1980-2022 for each 1.25 x 1.25 km grid cell in ESRI ArcGIS Pro 3.0.1. For each Daymet grid cell, we calculated the mean annual air temperature by averaging the annual maximum and minimum temperatures for each year, then computed the long-term average (1980-2022) for each grid cell. To derive ecoregion-scale climate summaries, we spatially averaged the long-term mean annual temperatures across all Daymet grid cells falling within each Level IV ecoregion where DPPs were located. The same steps were applied to average the precipitation.

3.2. Local scale analysis

To evaluate environmental, morphological and permafrost properties of DPPs, we undertook fieldwork at 3 sites within the central Mackenzie Valley: MM-1 (65.2244, -128.2825), FGH-1 (66.0094, -128.0899), and FGH-2 (66.0109, -128.0372). We drilled boreholes to a depth of ~3 m at MM-1, FGH-1, and FGH-2 using a portable permafrost coring system (Figure S2 in Supporting Information S1). The cores were sent to the Permafrost ArChives Science laboratory (PACs Lab) at the University of Alberta for preparation, description, and analysis.

Gravimetric water content (GWC), excess ice content (EIC), and frozen bulk gamma density were calculated following Pumple et al. [48], with gamma density obtained using a Geotek MSCL and ^{137}Cs gamma source. Conductivity and pH were measured using a Mettler Toledo SevenExcellence S470 Benchtop Meter. Water stable isotope ratios ($\delta^{18}O$, $\delta 2H$) were measured every 10 centimeters from pore water of thaw samples using a Picarro L2130-i water isotope analyzer. Raw isotope ratios were normalized to the Vienna Standard Mean Ocean Water-Standard Light Antarctic Precipitation (VSMOW-SLAP) using certified water reference standards (USGS-45 and USGS-46). $\delta^{18}O$ and $\delta 2H$ were used to detect isotopically depleted

horizons and identify potential thaw unconformities, thereby evaluating whether thaw had occurred during the Holocene at these sites. Following Lacelle et al. [49], we calculated the enrichment factor ($\varepsilon^{18}O_{i\text{-}w}$, ‰) between ice and water, hypothesizing that values within the equilibrium fractionation range (2.8‰ to 3.1‰) reflect thaw-refreeze processes. In contrast, values below this range suggest the absence of such isotopic exchange, indicating that peat plateaus surrounded by unfrozen channelized fens had remained frozen.

To reconstruct the genesis in which DPPs have formed, seven samples of 3 cm^3 were cut from each peat profile marked by stratigraphic changes and appearance of the peat. Vegetation composition was determined through analysis of plant macrofossils, focusing on three areas of the peat deposit: base, mid-core, and near-surface. Samples were treated with boiling 5% KOH solution and washed through a 42.5 µm sieve. Relative abundance was calculated as the percentage of total macrofossil count. Samples of plant macrofossils, with a preference for *Sphagnum* stems and leaves, were selected for ^{14}C dating to establish peat inception and to determine the ages of the deposit relative to depth and environmental parameters. Samples were prepared at the University of Alberta following standard acid-base-acid pretreatment, with solutions heated to 70 C: 30 min in 1 M HCl, 60 min in 1 M NaOH, changing the solution until clear, 30 min in 1 M HCl, and rinses with ultrapure water until neutral. Three secondary standards were also pre-treated concurrently for control: a last interglacial non-finite wood (AVR-PAL-07), a sub fossil wood (*Picea sp.*) (IAEA-C5), and a middle Holocene wood (FIRIF) (**Supplementary Table S1**). Samples were then dated at the Keck–Carbon Cycle AMS facility (University of California, Irvine). Radiocarbon dates were calibrated using the IntCal20 calibration curve [50]. Bayesian age-depth models were created by combining all dates into a P_Sequence model in OxCal v.4.4 [51]. The carbon-to-nitrogen (C/N) ratio was used to evaluate peat decomposition rates and infer permafrost aggradation history [52]. Samples were collected at 10 cm intervals and analyzed for total carbon and nitrogen by the Natural Resources Analytical Laboratory at the University of Alberta. We hypothesized that frozen peat would exhibit relatively moderate and consistent C/N ratios throughout the profile, indicating limited decomposition due to syngenetic permafrost aggradation during the Holocene.

Permafrost distribution and thickness were assessed using Electrical Resistivity Tomography (ERT) surveys conducted with an ABEM Terrameter L2. Each ERT measurement consisted of 1–4 stacked, with an acquisition time of 0.6 s per stack. Electrode positions were recorded using a Garmin inReach Explorer+ (±5 m horizontal accuracy), allowing accurate georeferencing of transects in ArcGIS. Frost table depth was measured at each electrode location using a 1.25 m probe for direct comparison with inverted resistivity models. Data were inverted in RES2DINV [53] using default settings with L2 norms applied to both data and model misfit, and a regularization parameter of 0.15 following Herring et al. [54].

4. Results and Interpretation

4.1. Regional distribution of DPPs

Dendritically-drained peat plateaus were mapped across the study area to explore geological and terrain factors controlling the distribution (**Figure 1a**). We identified 14,784 grid cells (1.25 x 1.25 km) containing DPPs, covering approximately 22,500 km². DPPs are distributed across fluted till plains of the southern and Central Mackenzie valley, and become less common in the northern Taiga Plains and low-subarctic region. The till plains that host DPPs are characterized by slopes less than 0.30° (σ = 0.37), with examples of some networks forming on slopes of up to 1.5° near the Mackenzie Mountains or the Horn Plateaus (**Figure 1a; Figure S3 in Supporting Information S1)**. They are mapped across terrain ranging from 20 m to 860 m a.s.l., with a median elevation of 238 m a.s.l. (μ = 276 m a.s.l., σ = 141), occurring outside the glaciolacustrine plains associated with the ancient proglacial Lake Mackenzie (**Figure 1a**) [31]. No DPPs were identified north of Great Bear Lake (Colville Lake) or along the NWT–Nunavut border, nor in the Boreal Cordillera and or in the Mackenzie Mountains, dominated by bedrock outcrops and lesser organic terrains (**Figure 1a**). Our detailed mapping using high-resolution imagery, compared with NWT-wide permafrost and thermokarst feature mapping [43], indicates 81% agreement.

DPPs in the Taiga Plains occur across a mean annual air temperature (MAAT) range of –2.5°C to –7.5°C, with an overall mean of –4.9°C (σ = 0.8) (**Figure S3 in Supporting Information S1**). Air temperatures generally decrease northward, though local variation is evident. In the southern Taiga Plains, average MAAT typically ranges from –2.5 to –3.5 °C and is associated with

298 relatively thin permafrost; however, colder conditions (~–5 °C) are also recorded at higher-
299 elevation southern sites. These colder temperatures are comparable to those observed at higher
300 latitudes, highlighting the influence of elevation on regional climate patterns. Mean annual
301 precipitation across the region averages 350 mm (σ = 81), with most sites (57%) receiving
302 between 300 and 400 mm yr^{-1}. A clear latitudinal gradient is evident, with generally drier
303 conditions (≤300 mm yr^{-1}) in northern regions and higher precipitation toward the south,
304 reaching a maximum of ~675 mm on the Horn Plateau area, which also represent our highest
305 elevation sites (**Figure 1a; Figure S3 in Supporting Information S1**).

306 **4.2. Geophysical characteristics and permafrost configuration**

307 A subset of these distinctive DPP assemblages in the central Mackenzie Valley was investigated
308 using ERT to assess contrasting surface and subsurface conditions between elevated, frozen peat
309 plateaus, internally affected by unfrozen collapse scars, and the surrounding unfrozen
310 channelized fens (**Figure 2**).

311 The first site, MM-01, near the Mackenzie Mountains foothills (~384 m a.s.l.), is an open
312 black spruce site with a ground cover of reindeer lichen (*C. stellaris*), *Sphagnum fuscum*, and
313 feathermosses (*P. commune*, *D. groenlandicum*) (**Figure 2a**). The 4-m-spacing ERT survey started
314 on a peat plateau, crossed two narrow channelized fens (14 and 6 m) separated by a small peat
315 plateau (10 m), then traversed a large 66-m-wide peat plateau, passed through a collapse scar
316 (15-m wide), and terminated on the same peat plateau. The ERT profile shows high resistivity
317 values under the peat plateaus, and based on the sharp transition between low and high
318 resistivity, the thickness of permafrost is estimated at 5 to 9 m. Low resistivity values (<300 Ω·m)
319 correspond to unfrozen ground and match the location of the channelized fens and bogs crossed
320 by the survey (**Figure S4 in Supporting Information S1**).

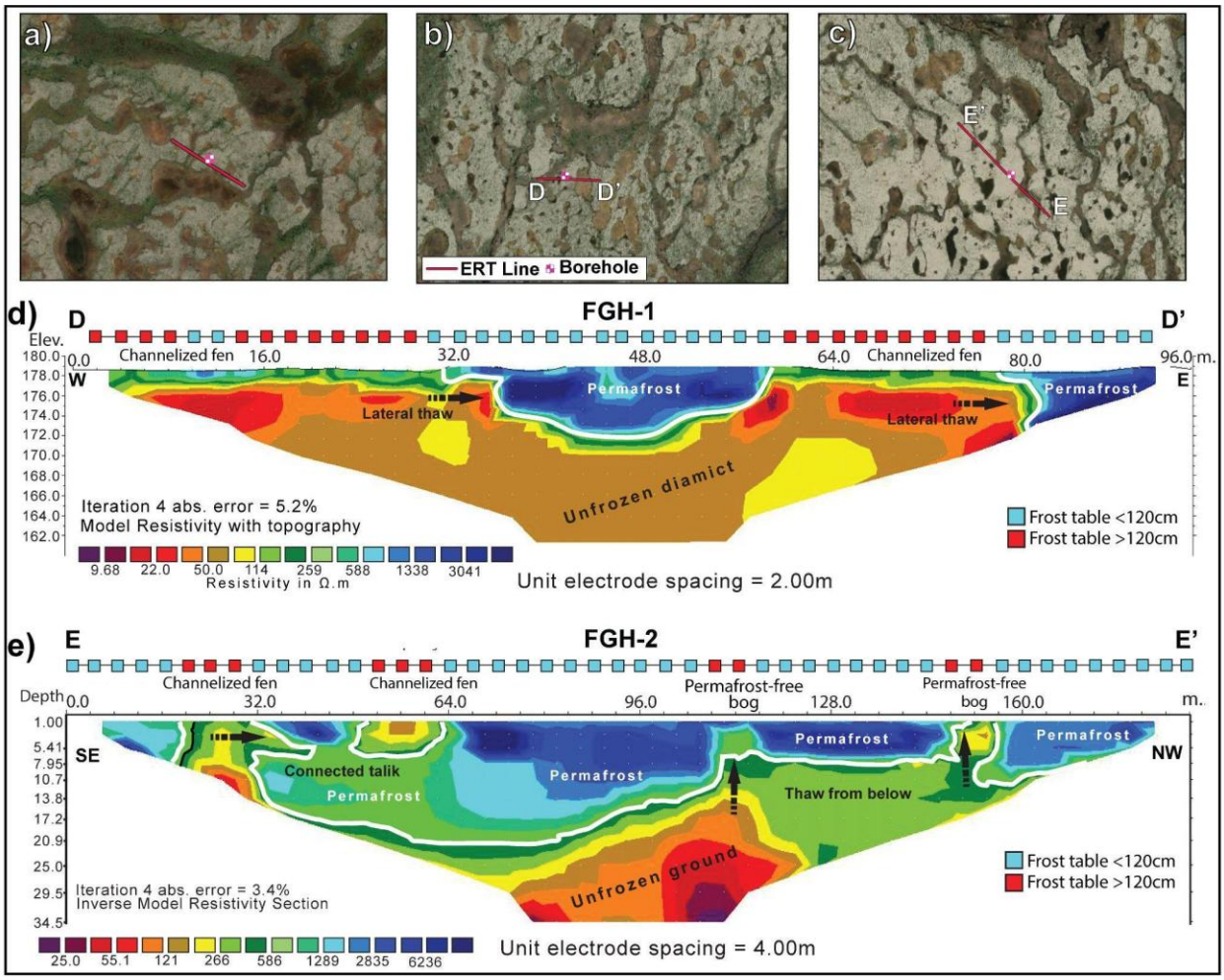

Figure 2. High-resolution imagery (a-c) of studied dendritic peat plateaus with channelized fens, collapse scars and raised peat plateaus, a) MM-1, b FGH-1 & c) FGH-2, with ERT surveys completed in June 2022 and boreholes location. Electrical resistivity tomography surveys in June 2022 showing profiles across at d) FGH-1 and e) FGH-2 with inferred permafrost boundaries (white lines) and frost table measurements.

FGH-1 is located on a till plain covered with *Cladonia* subg. *Cladina stygia* and *Flavocetraria cucullata*, open black spruce, and low shrubs at an elevation of ~178 m a.s.l. The ERT survey (2-m spacing) began in a large channelized fen (74 m), crossed a 30-m wide peat plateau, and crossed a second channelized fen (20 m) to end in a second peat plateau (**Figure 2b**). Frost probing was carried out along the survey and indicated the absence of permafrost within the upper 120 cm in the channelized fens, and the frost table reaching less than 40 cm over the peat plateaus. Profile FGH-1-A shows high-resistivity values (≥300 Ω.m) under the 30-m width peat plateau, suggesting permafrost extends to depths of 5-7 m (**Figure 2d**). The two

channelized fens are underlain by low resistivity (≤300 Ω.m), reflecting the presence of unfrozen ground and taliks.

Located 2 km east of FGH-1 and at the top of the drainage system, FGH-2 (~184 m a.s.l.) is part of the same dendritically-drained peat plateau complex, but the site is more open with sparse black spruce near the outlet and a ground cover dominated by reindeer lichens. The channelized fens are narrower, and fewer internal collapse scars were observed near the site compared to FGH-1 (**Figure 2c**). The survey (4 m spacing) started on a peat plateau, crossed a narrow channelized fen twice, a large peat plateau, and then crossed two small collapse scars before finishing on a peat plateau. The 44 m-wide permafrost peat plateau is characterized by high resistivity values (≥300 Ω·m) extending to depths to ~20 m, indicating permafrost thickness. The narrow intertwining channelized fens (14-17 m) and small collapse scars (<8 m) were underlain by lowest resistivity values (≤300 Ω.m), indicating taliks (**Figure 2e**). Unfrozen ground to depths greater than 120 cm was confirmed by probing the collapse scars and channelized fens.

4.3. Stratigraphy and Paleoecology of DPPs

Frozen cores were collected on permafrost peat plateaus to depths of 3 m from DPPs in the central Mackenzie Valley to characterize soil properties, permafrost formation, and their development history. The stratigraphies are about 2 m of structureless organic-rich peat overlying an ice-rich diamict with lenticular, reticulate, and crustal cryostructures, composed of ice lenses ranging from several millimeters to 10 cm thick **(Figure S2 in Supporting Information S1)**. Gravimetric water content and excess ice content vary substantially across the profile. In the peat, GWC ranges from 267% to 1642% at MM-1 and 120% to 1212% at FGH-2. In the diamict, GWC ranges from 20% to 2359% at MM-1 and 19% to 183% at FGH-2, with EIC ranging from 0% to 93% (μ = 16%) and 0% to 58% (μ = 22%), respectively (**Figure 3a-b**).

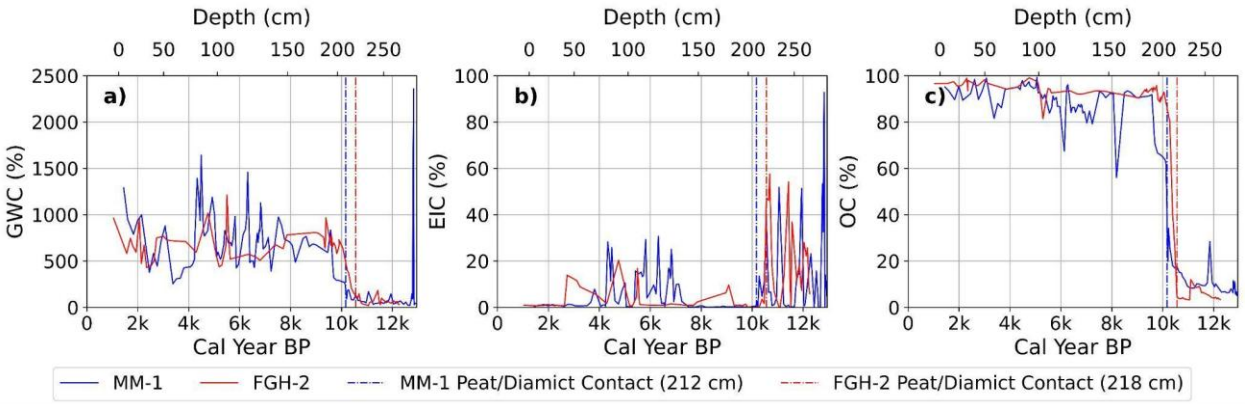

Figure 3. Stratigraphic parameter variations shown by radiocarbon (cal yr BP, ^{14}C) age-depth models for MM-1 and FGH-2, and by depth. Parameters include A) gravimetric water content (GWC %), B) excess ice content (EIC %), C) organic carbon content (OC %). Red and blue lines represent environmental parameters from FGH-2 and MM-1, respectively. Dash-dot vertical lines indicate the peat/diamict stratigraphic contact for each core (MM-1: 212 cm; FGH-2: 218 cm).

Particle size distributions indicate that the diamict for both sites is mainly composed of silt (36-76%), with clay (6-46%) and sand (0.4-58%) (**Figure S5 in Supporting Information S1**). The transition from peat to diamict is delineated by gamma density and organic content (OC) measurements, with gamma density averaging 0.95–0.97 g/cc in the peat (<220 cm) and increasing to 1.44–1.50 g/cc below ≥220 cm, while OC decreases from 86–90 % in the peat to 5–10 % at the same depth (**Figure 3c; Figure S6a in Supporting Information S1**).

Radiocarbon dating indicates that peatland initiation occurred during the early Holocene. At MM-1, basal peat at 219 cm dates to 10,195 cal yr BP, whereas at FGH-2, basal peat dates to 10,040 cal yr BP. At FGH-1, basal peat at 133 cm dates to 3,289 cal yr BP, suggesting a much later initiation at this site. At MM-1, unidentified plant material within the underlying diamict at 280.5 cm below ground surface indicate an age of 12,773 cal yr BP (**Table 1**; **Figure S7 in Supporting Information S1**). These ages align with the timing of ice retreat [33], formation of the glacial lake Mackenzie [31] and subsequent vegetation shifts [16], as indicated in the plant macrofossil record, marking the transition from barren soil surfaces from permafrost-free environment to peat accumulation with permafrost.

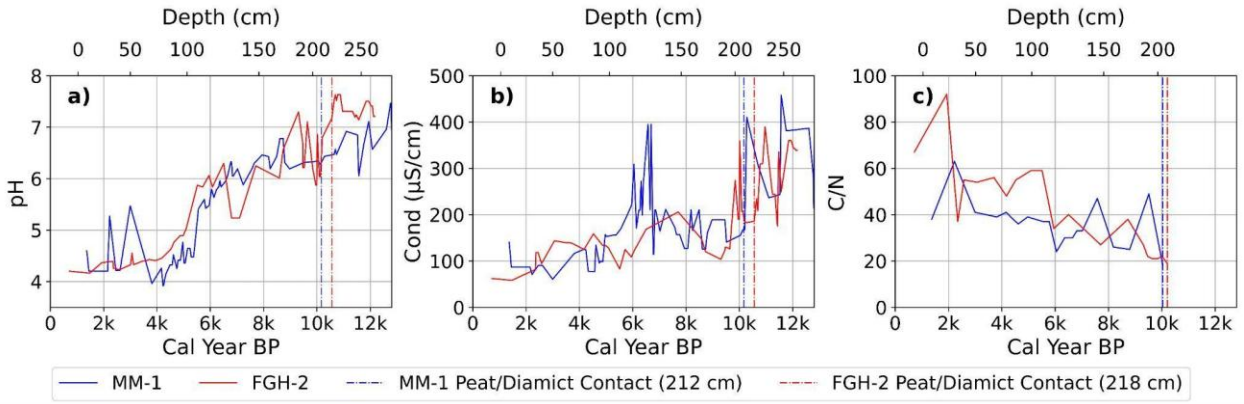

Figure 4. Environmental parameter variations shown by radiocarbon (cal yr BP, ^{14}C) age-depth models for MM-1 and FGH-2, and by depth. Parameters of pore ice waters include A) pH, B) conductivity (µS/cm), C) C/N ratio.Red and blue lines represent environmental parameters from FGH-2 and MM-1, respectively. Dash-dot vertical lines indicate the peat/diamict stratigraphic contact for each core (MM-1: 212 cm; FGH-2: 218 cm).

Vegetation composition shifts from minerotrophic (ground water source) to ombrotrophic (atmospheric water source) environments as peat accumulation progresses. Basal peat layers were dominated by bryophytes such as *Sarmentypnum exannulatus* and *Scorpidium scorpioides*, suggesting a hydrophytic environment with higher pH (5.8-6.5) and conductivity (200-457.7 µS/cm) from pore ice waters. Upper peat layers, however, are dominated by *Sphagnum* spp. (e.g., *S. girgensohnii* and *S. fuscum*), with pH values as low as 3.9 and conductivity below 100 µS/cm, indicating ombrotrophic and nutrient-poor conditions (**Figure 4a-b**).

Changes in C/N ratios and stable isotope composition (δD vs. $\delta^{18}O$) can indicate decompositional environments and thaw-refreeze processes in permafrost landscape. At MM-1 and FGH-2, C/N ratios ranged from 18 to 63 and 19 to 92, respectively. The highest values were found in the active layer (38–63 at MM-1; 56–92 at FGH-2), indicating limited decomposition and a higher proportion of labile carbon. In contrast, below this depth, C/N ratios were more moderate and stable (18–49 at MM-1; 19–38 at FGH-2), consistent with long-term carbon preservation under syngenetic permafrost aggradation (**Figure 4c**). At MM-1, $\delta^{18}O$ values range from –19 to –21‰ and δD from –150 to –163‰, with d-excess values of +4 to +6‰. The linear regression of δD vs. $\delta^{18}O$ yields a slope of 6.66 (R^2 = 0.82) with an intercept of –23.2. Enrichment fraction **(**$\delta^{18}O_{i-}w$) values range from 0.78 to 1.82‰. In contrast, FGH-2 exhibits $\delta^{18}O$ values between –18.9 and –20.91‰, with d-excess values from –2 to –4‰. The δD–$\delta^{18}O$ regression

slope is 7.87 (R^2 = 0.98), slightly steeper than the local meteoric water line (**Figure S6 in Supporting Information S1**).

TABLE 1. Radiocarbon dates, and calibrated ages from the three dendritic peat plateaus profiles in the central Mackenzie Valley.

Core name	Sample Depth (CM)	Material	Sample ID	^{14}C age (yr BP)	±	Median age (cal. yr BP)	Calibrated 2s distribution (cal. yrBP range, %)
FGH-2-2	49.5	*Sphagnum* stems	UCIAMS- 265212	2360	15	2353	2414-2385, 7.7%; 2370-2340, 87.7%
FGH-2-5	115.5	*Sphagnum* stems	UCIAMS- 265213	4795	15	5512	5588-5550, 24.9%; 5538-5477, 70.5%
FGH-2-7	156.5	*Sphagnum* stems	UCIAMS-265214	8290	20	9307	9419-9341, 38.1%; 9334-9202, 44.8%; 9178-9142, 12.6%
FGH-2-8	200.5	Wood fragment	UCIAMS-274831	8910	25	10,039	10,180-10,110, 28.7%; 10,089-9909, 66.7%
FGH-1-3	85.5	*Sphagnum* stems	UCIAMS-265215	2305	15	2340	2353-2315, 95.4%
FGH-1-5	133.5	*Sphagnum* stems	UCIAMS-265216	3065	15	3289	3349-3218, 95.4%
MM-1-2	60.5	*Sphagnum* stems	UCIAMS- 274830	3830	15	4202	4342-4339, 0.4%; 4293-4151, 95.1%
MM-1-6	151.5	Wood fragment	UCIAMS-265217	5975	15	6810	6882-6870, 3.5% 6855-6743, 91.9%
MM-1-9 A .18mgC	212.5	*Sphagnum* stems	UCIAMS-265218	8995	30	10,194	10239-10142, 88.4%; 10060-10043, 2.2%; 9987-9964 4.8%
MM-1-9B	280.5	Plants Unknown	UCIAMS-292560	10,860	25	12,773	12,828-12,743, 95.4%

4.4. Variation in DPP Landform Assemblage Morphology

To explore variation in DPP morphology, we manually mapped these landform assemblages (n=398; total area = 2,058 km²) across six Level IV ecoregions spanning the latitudinal and ecoclimate gradients of the Taiga Plains: Bulmer Plain (LS), Carcajou Plain (LSb), Blackwater Upland (LS), Horn Plateau (LS), North Mackenzie Plain (LS), and Arctic Red Plain (HS) (**Figure S8 in Supporting Information S1**). These ecoregions were selected to capture the full range of environmental conditions influencing DPP development, including difference in elevation, slope, air temperature, and Holocene history.

4.4.1. Morphological variance

DPP basin areas ranged from 0.19 to 45.0 km² (μ = 5.4 km², σ = 7.1 km²). It varied significantly among ecoregions (Kruskal–Wallis H = 134.2, $p < 0.001$), ranging from 2.1 ± 2.4 km² in the Carcajou Plain to 15.2 ± 11.6 km² in the Bulmer Plain, representing an approximately seven-fold difference in mean basin size. Further, basin morphology was classified as elongated (36.4%), intermediate (62.8%), or circular (0.8%) based on morphometric thresholds. DPP shape varied significantly among ecoregions, with elongated basins significantly larger than intermediate basins (6.7 ± 8.4 vs. 4.6 ± 6.1 km²; Mann–Whitney U = 19,164, p = 0.0014) and occurred on gentler slopes (Mann-Whitney U = 12,324, p = 0.0002). Basin morphology class distribution varied significantly among ecoregions ($\chi^2 = 22.11$, p = 0.0005), ranging from 20% elongated in Carcajou Plain to 55% in Blackwater Upland. R_e ranged from 0.15 to 0.92 (μ = 0.63, σ = 0.11), while C_c ranged from 1.23 to 2.98 (μ = 1.80, σ = 0.33) (**Figure 5b-c**). The Carcajou Plain ecoregion exhibited the most compact DPPs, characterized by low C_c (1.60 ± 0.18) and relatively high R_e (0.68 ± 0.10), followed by the Horn Plateau (C_c = 1.64 ± 0.27, R_e = 0.66 ± 0.12). In contrast, DPPs in the Bulmer Plain showed the most elongated and irregular forms, reflected by higher C_c (2.04 ± 0.35) and lower R_e (0.63 ± 0.10), with similarly elongated morphologies observed in the Arctic Plain and Blackwater Level IV ecoregions (C_c = 1.94 ± 0.34, R_e = 0.64 ± 0.11; C_c = 1.82 ± 0.29, R_e = 0.59 ± 0.10, respectively) (**Figure 5b-c**). These patterns reflect regional differences in valley confinement and influence on DPP morphology. More compact (i.e., more circular) basins are commonly associated with steeper terrain (**Figure 1d-6b**), whereas elongated basins promote linear drainage along gentle gradients (**Figure 1b,c,e-6b**). Basin relief did not differ significantly between shape classes (33.3 ± 68.0 vs. 27.2 ± 21.4 m; U = 16,567, p = 0.56), suggesting that other factors such as ground ice, precipitation, or organic extent may control DPP morphology.

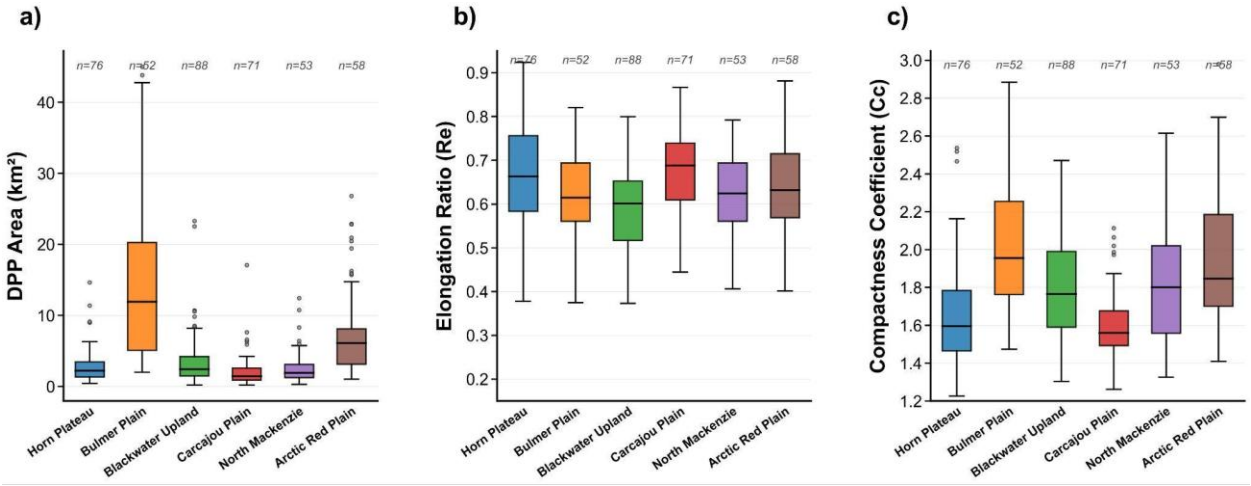

Figure 5. A) Cumulative total area of DPPs; B) Elongation Ratio (Re), with lower values indicating more elongated basins; C) Compactness coefficients (Cc) with higher values indicating more irregular shapes.

4.4.2. Regional Climate Variability and Collapse Scar/Fen Characteristics

Regional climate gradients strongly influence DPP morphology and distribution. The Bulmer ecoregion is low-lying (slope = 0.11°; σ = 0.07°) and poorly drained (**Figure 6a,b**) with the warmest mean annual, summer and winter air temperatures (–5.37°C; σ = 0.39) of all regions sampled in this study (**Figures 6c, 8**). In contrast, the elevated, and better-drained (slope = 0.42; σ = 0.22) (**Figure 6a,b**) Horn Plateau LS ecoregion has significantly greater proportion of frozen peat plateaus relative to collapse scars/fen coverage, with narrower channelized fens (μ = 34.5 m, σ = 26 m) and smaller collapse scars and basins (**Figures 6-7**) than the Bulmer Plain. The mean annual air temperatures of the Horn Plateau LS (–5.4°C) are two degrees lower than the adjacent Bulmer Plain (–3.6°C), and the greater regional slope reflects better drainage conditions (**Figure 6a-c**). The Blackwater Upland LS occupies an intermediate position with moderate elevation (μ = 382 m, σ = 74 m) and well-drained terrain (slope = 0.40°; σ = 0.23°), experiencing cold temperatures (-5.1°C; σ = 0.49°C) that maintain moderate channelized fen widths (μ = 85 m, σ = 52 m) and a relative similar proportion of collapse scar/fens and peatlands (**Figures 6-7**). Despite similar poor drainage conditions (slope = 0.35°; σ = 0.21°), the Carcajou Plain LSb shows smaller collapse scars (μ = 330 m², σ = 195 m²) and narrower fens (μ = 58 m, σ = 27 m) than the Bulmer Plain, as colder temperatures (–5.3°C; σ = 0.33°C) and limited precipitation (μ = 365 mm, σ = 15 mm) maintain permafrost stability (**Figure 6c-f**). The North Mackenzie Plain LS (slope = 0.21°; σ = 0.13°)

represents continental conditions, where cold temperatures (–5.1°C) and minimal precipitation (305 mm) override poor drainage to maintain narrow channelized fens (μ = 38 m, σ = 18 m) and minimal collapse scars (μ = 125 m², σ = 68 m²) (**Figure 6a-f**). However, the increase in the proportion of collapse scars/fens, as well as fen width (μ = 52 m, σ = 27 m) and collapse scar size (μ = 485 m², σ = 390 m²), in the northernmost Arctic Red Plain (**Figure 6e,f-7**) can be attributed to the lower slope of the low-lying (slope = 0.14°; σ = 0.09°), poorly drained permafrost peatlands, despite it being the coldest (–5.6°C; σ = 0.31°C) and driest ecoregion (260 mm) we sampled in this study (**Figure 6c-d**). The poorest drainage conditions and aridity of this northernmost ecoregion override the cold temperature controls on permafrost/collapse scar/fen distribution leading to an increase in these thawed areas than the intermediate ecoregions.

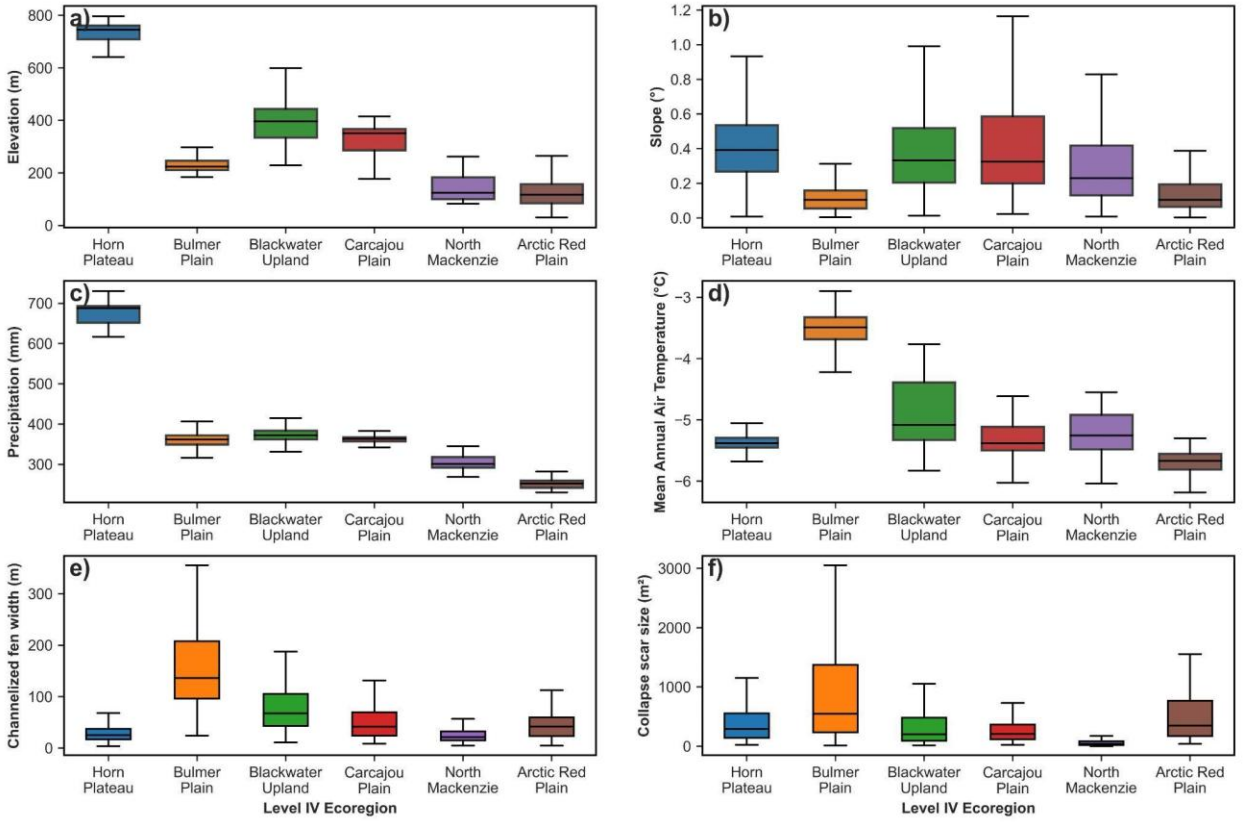

Figure 6. Boxplots showing the climate and morphological parameters of DPPs across six Level IV ecoregions of the Taiga Plains: (A) elevation (m a.s.l.), (B) slope (°), (C) mean annual air temperature (°C), and (D) annual precipitation (mm), E) measured width in channelized fen across different ecoregions, and the F) measured size of collapse scars and basins within DPPs per ecoregions.

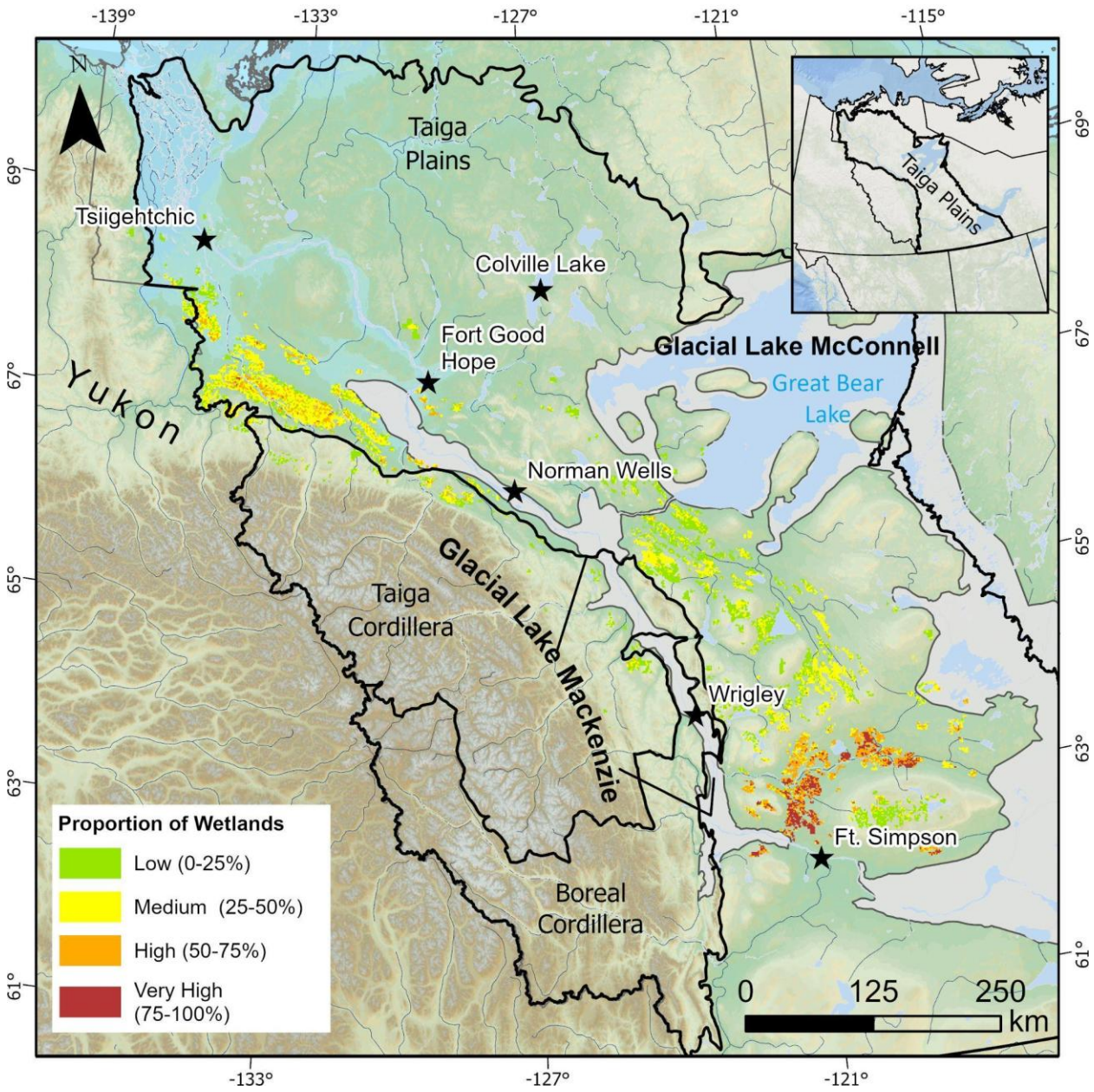

Figure 7. The proportion of channelized fens and collapse scars within DPPs per grid cell (1.25 x 1.25 km) from low (0-25%), medium (25-50%), high (50-75%), and 4) very high (75-100%).

5. Discussion

5.1. Distribution and morphological variation

The broadscale distribution of DPPs reflects the intersection of geological inheritance, climate conditioning, and ecological development that characterizes permafrost landsystems [23]. The occurrence of DPPs in poorly drained organic terrain where thick organic deposit mantle extensive drumlinied till plains with low-relief (< 0.30°) above the limits of ancient glacial lakes indicates that substrate characteristics and slope are primary controls on the landsystem development. The absence of DPPs in eastern NWT and along the NWT-Nunavut border is attributed to the lack of extensive organic deposits in these areas [1,43]. DPPs are most common in the Taiga Plains where sedimentary bedrock is buried beneath thick fine-grained till deposits, creating vast, poorly-drained landscapes, allowing for the development of large organic deposits with permafrost [1,16]. The same holds for the glaciolacustrine plains lowlands areas of the central Mackenzie Valley, where only few DPPs have been identified, likely reflecting limited conditions for peat accumulation and dendritic drainage pattern development. In these environments, ramparted lake-lithalsa complexes, abundant lakes and wetlands, segregated ice, and undulating topography preclude the development of dendritic peatlands [43].

The latitudinal gradient in DPP morphology demonstrates how climate and basin shapes conditioning landsystem expression, with warmer temperatures in southern regions. There, DPPs are characterized by larger channels, collapse scars, and greater fens connectivity (**Figure 1b-6e-f**). The higher thermal conductivity of wet peat accelerates permafrost thaw, especially when combined with fire events [5,55] as indicated by the high proportion of collapsed scars and channelized fens in the areas. DPPs in the Level IV Carcajou Plains and Horn Plateau ecoregions have more isolated collapse scars, smaller channelized fens and intact permafrost features (**Figure 6e-f**). The data indicate that slope and temperature interact to dictate the balance between collapsed scars/fens and peat plateaus, where steeper slopes and colder conditions favor narrower channelized fens and better drainage. These differences in morphology and climate parameters suggest that DPPs in colder, higher-slope environments may have different trajectories of change compared to southern counterparts. In contrast, DPPs in the colder Arctic

Red Plain ecoregion have thicker organic deposits, may host more ground ice, and are characterized by ice-wedge polygon networks (**Figure S9 in Supporting Information S1**), which may lead to a different thaw trajectory.

In the Taiga Plain ecozone, basin geometry, permafrost and topographic constraints influence drainage organization and network complexity [56]. These controls on hydrology and channel development are reflected in DPPs of the Taiga Plains, which exhibit distinct basin morphologies that vary in size, shape, and drainage density. These observations indicate that the interplay of topography, basin geometry, and permafrost extent governs DPP morphology, with higher-elevation, topographically constrained areas (e.g., between till plains) producing smaller, more circular basins (**Figures 6-7**), while lower-relief regions allow for larger, more elongated and linear drainage networks to develop (**Figures 6-7**).

5.2. Evolution of DPPs during the Holocene

Peatlands in the Taiga Plains provide insights into postglacial landscape evolution. Basal peat ages (~10,000 cal yr BP) are consistent with previously reported dates from the central Mackenzie Valley [16] and align with the timing of glacial lake drainages [31,32,34]. Glaser [26] proposed two models of formation for the streamlined bog island, which are conceptually similar to DPPs. The first model involves flow obstructions influenced by bedrock outcrops, and the others by fragmentation of a continuous bog into islands by developing water tracks. Large bogs can develop their own internal drainage networks. A supply of alkaline groundwater near the bog crest can alter the vegetation, transforming bogs into fens that result in a different type of peat development. The interaction between these alkaline waters and the surrounding bog vegetation then form streamlined bog islands. Similarly, DPPs exhibit dendritic drainage networks where channelized fen features develop along preferential flow paths, and variations in wetness influence permafrost aggradation and development of a peat plateau, reinforcing drainage patterns. Variation in patterns and proportion of peat plateau, fen networks and collapse basins vary with climate-driven permafrost distribution, modulated by slope and hydrological conditions. Based on our broadscale mapping, morphological assessments, geophysical and

536 drilling field investigations, we propose the following sequence for DPP development in
537 permafrost:

538 1) Macrofossil analyses indicate that peatland development began in a hydrophytic
539 environment with mineral-rich water influence. Channelized fens or streams likely predated peat
540 plateau formation, with dendritic drainage patterns forming on gently sloping terrain prior to
541 permafrost aggradation (**Figure 8a**).

542 2) Peat accumulation at the site (initially *Sphagnum* spp.) led to permafrost aggradation
543 at drier interfluves, accompanied by the growth of segregated ice lenses as permafrost aggraded
544 through the peat-mineral interface, causing upward displacement of the peat surface due to frost
545 heave. This progressively dried the peat surface over time and transitioned communities from a
546 wetland (*Sphagnum exannulatus* and *S. scorpioides*) to drier conditions (*Picea sp., Sphagnum spp.*
547 and then *Cladina sp.*) after permafrost elevated the surface [57]. Peat fibers were moderately
548 well preserved throughout the profile at both sites, suggesting rapid permafrost aggradation
549 around 8-7 ka BP (**Figure 4c**; **Figure S4 in Supporting Information S1**). Isotopic data provide
550 additional evidence for early permafrost aggradation and the long-term stability of segregated
551 ice at both sites. At MM-1, relatively low and consistent $\delta^{18}O_{i\text{-}}w$ enrichment values, along with
552 well-preserved peat fibers and the absence of isotopic discontinuities, suggest continuous and
553 undisturbed permafrost since at least 8–7 ka BP (**Figure S6b in Supporting Information S1**). This
554 suggests that MM-1 may have remained perennially frozen throughout the Holocene. In contrast,
555 FGH-2 shows greater isotopic variability and higher $\delta^{18}O_{i\text{-}}w$ enrichment, consistent with more
556 dynamic freezing conditions likely influenced by intermittent thaw or water movement. None of
557 the cores from either site exhibit $\delta^{18}O_{i\text{-}}w$ values within the 2.8 to 3.1‰ range identified by Lacelle
558 et al. [49] as indicative of thaw unconformities and subsequent permafrost re-aggradation
559 (**Figure S6c in Supporting Information S1**).

560 3) Permafrost peat plateaus likely formed throughout the cooling Holocene, maintaining
561 a relative equilibrium between frozen ombrotrophic bogs and unfrozen ground in the
562 minerotrophic channelized fens depending on the regional climate and drainage. During cooler
563 or drier periods, it is plausible that peat plateaus increased in aerial extent expanding toward
564 channelized fens reducing unfrozen areas, while during warmer, wetter intervals, channelized

565 fens and collapse bogs may have expanded dissecting raised peat plateaus and increasing the
566 proportion of unfrozen areas within the DPPs (**Figure 8b**).

567 Recent warming and increasing ground temperatures in recent decades [2, 58] has
568 decreased permafrost extent across frozen peatlands in the Western Arctic region [9,59,60]. In a
569 warming climate, widening of channelized fens may now be enhanced by advective heat transfer,
570 creating a positive feedback: as fens expand, increased water flow accelerates thawing and
571 fragmentation further expanding channelized fens (**Figure 8c**).

572 A next step would be to collect macrofossil samples from the largest unfrozen channelized
573 fens to further test this interpretation. While more recent and smaller channelized fens are
574 typically the result of permafrost degradation through lateral and internal thaw, the origin and
575 longevity of larger channelized fens remain uncertain. Detailed macrofossil analysis could provide
576 information into whether frozen peatlands and adjacent unfrozen channelized fens have
577 coexisted in a dynamic equilibrium throughout the Holocene. This would contribute to a more
578 comprehensive understanding of the long-term stability, resilience, and feedback mechanisms
579 governing permafrost–landscape interactions in peatland environments.

580 **5.3. Subsurface characteristics and permafrost configuration**

581 Electrical resistivity tomograph surveys show that DPPs in the central Mackenzie Valley are
582 underlain by permafrost less than 20 m thick beneath raised plateaus, while channelized fens and
583 larger collapse scars are underlain by talik **(Figure 4**). Permafrost thickness appears linked to the
584 spatial configuration of peat plateaus and surrounding channelized fens. At FGH-2, where peat
585 plateaus are wider (>50 m) and fens are narrower (<15 m) and more widely spaced, permafrost
586 reaches 20 m thickness. In contrast, at MM-1 and FGH-1, where peat plateaus are narrower (30-
587 50 m) and surrounded by wider channelized fens (30–80 m), permafrost is thinner (5-10 m).
588 These patterns suggest that within a climate region and also locally, larger intact peat plateaus
589 with reduced fen connectivity maintain thicker permafrost, likely due to reduced advective heat
590 transfer from groundwater flow.

591

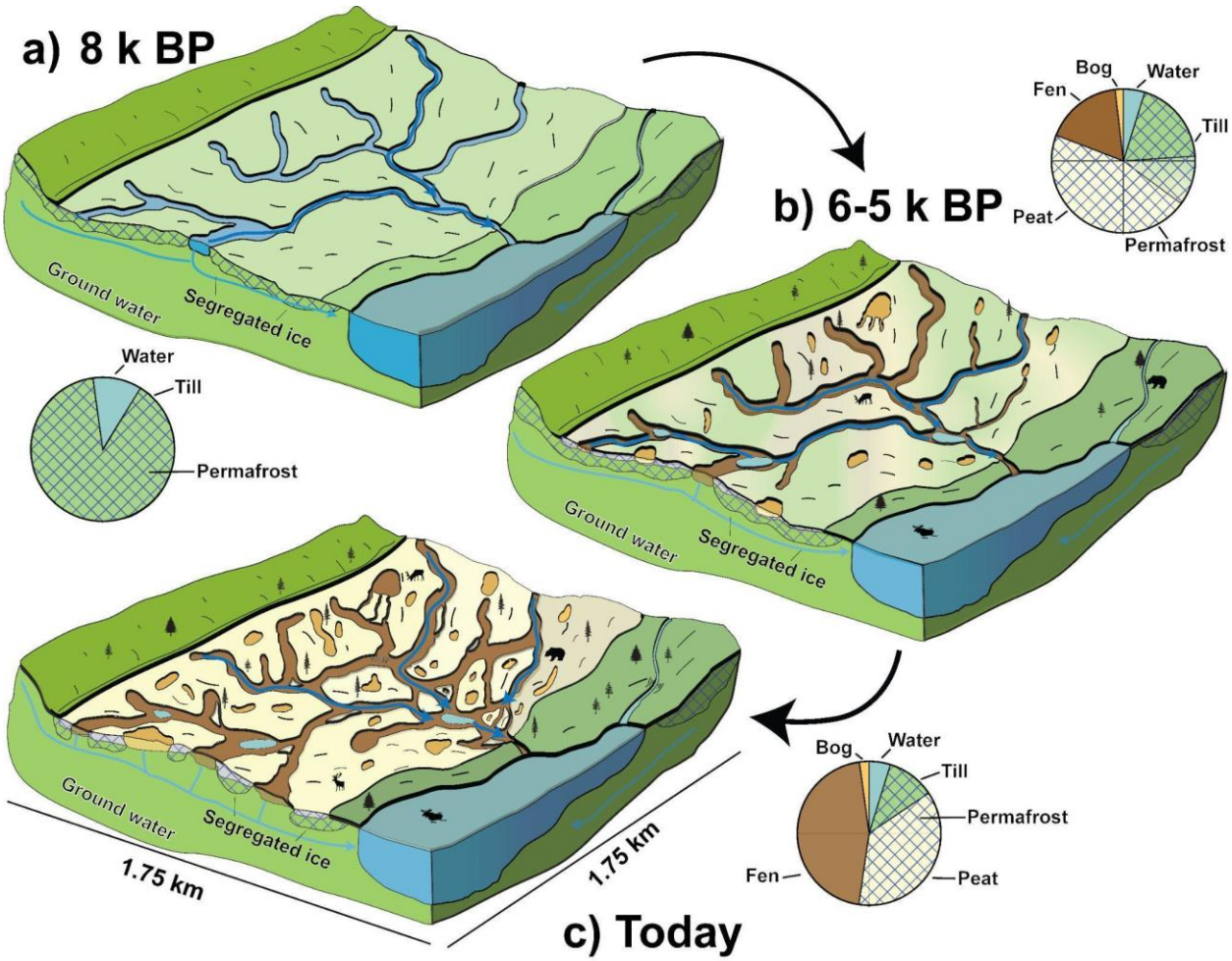

Figure 8. Conceptual representation of the formation of a dendritically-drained peat plateau (DPP) landsystem in the discontinuous permafrost zone, showing permafrost distribution and stratigraphy. Pale yellow = peat plateaus; green = till; blue = water; brown = fens; orange = collapse scars (bogs). a) Post-deglaciation landscape: permafrost aggrades near the surface and a dendritic fluvial network forms in homogenous substrate along the regional slope. b) Widespread permafrost aggradation in well-drained areas with initial accumulation of organic matter over till; early dendritically-drained peat plateaus start developing. c) Legacy channels now host unfrozen terrain in former dendritic fluvial pathways; expansion of channelized fens due to degradation of permafrost peat plateaus is accentuated during wet and warming periods; Relatively thin permafrost is present under raised peat plateaus.

Thick organic matter overlying diamict provides effective insulation, allowing frost to propagate into the ground and develop segregated ice lenses in the upper till deposit. Since the peat cover is relatively thick (~2 m), it offers important protection to the underlying ice-rich mineral soil. However, recent modeling experiments [61,62] suggest that peatland thawing commonly occurs by lateral thaw, extending beneath the peat, penetrating the underlying mineral soil and propagating into the peat plateau interior. This is consistent with our ERT data

609 showing lower resistivity values along fen margins extending into DPP interiors, suggesting lateral
610 heat transfer from unfrozen ground to below ice-rich diamict deposits (**Figure 3d-e**). The
611 proximity of water and ice-rich soil likely contributes to thermal undercutting and eventual block
612 erosion at margins or ground ice subsidence (**Figure 9a-b**). The arrangement of peat plateaus and
613 channelized fens, where permafrost and non-permafrost wetlands are in contact, suggests
614 significant lateral heat fluxes occur with important implications for permafrost stability.
615 Permafrost degradation is driven by the expansion of unfrozen ground from below, leading to
616 thermokarst depressions and vertical thaw processes that progress both upward from the base
617 and downward from the surface. Evidence of recent collapse scars without surficial perturbation
618 suggests that thaw from below may be driven by geothermal heat flux (**Figure 9c**). However,
619 lateral thaw rates are approximately an order of magnitude greater than vertical thaw rates.
620 Consistent with this, ~77% of the observed degradation is attributed to lateral talik expansion at
621 fen–peat plateau interfaces, whereas ~20% is associated with collapse scars expansion [63].

622 **5.4. DPPs as a Permafrost Landsystem**

623 The permafrost landsystem concept provides a framework for synthesizing our observations of
624 surface morphology and subsurface characteristics of DPPs and their spatial distribution across
625 the Taiga Plains ecozone (**Figure 8**). As defined by Kokelj et al. [23], a permafrost landsystem
626 integrates recurring patterns of landforms that co-develop with ecological communities,
627 together reflecting characteristic properties of soils, thermal conditions, ground ice distribution,
628 and ecosystems. Here we demonstrate that DPPs represent such an integrated permafrost
629 system.

630 The distinctive assemblage of raised permafrost plateaus dissected by dendritic
631 channelized fens reflects the interplay between geological inheritance (predominantly till
632 deposits), climate conditioning (through the Holocene), hydrology, and ecological development.
633 The recurring arrangement of these components, and permafrost-ecological feedbacks that
634 occur across the northern Taiga Plains indicates a set of processes governing landsystem
635 evolution. The systematic variation in DPP expression along latitudinal and elevational gradients

636 further illustrates how climate interacts with hydrology and vegetation to influence permafrost
637 landsystem characteristics.

638

639 **Figure 9.** Photographs showing permafrost degradation features. (A) Channelized fen incision
640 through peat plateau with thermokarst depressions and Reindeer lichens. (B) Block erosion along
641 channel fen margins with exposed substrate. (C) Active layer thaw features and vegetation
642 transitions from lichen- to moss/sedge-dominated communities indicating recent permafrost
643 degradation.
644

This landsystem approach offers several advantages for understanding permafrost terrain. First, it provides a scale-appropriate framework for translating between site-specific permafrost observations (configuration, temperatures, and ground ice) and regional patterns. Second, it connects the physical configuration of landforms to ecological processes and hydrological function. Third, it enables prediction of how these systems may respond to climate change based on their intrinsic properties.

The sensitivity of DPPs to climate warming varies regionally, with southern examples showing higher collapse scars/fens proportions than northern counterparts. However, some of these unfrozen wetlands may not be attributable to thermokarst processes (e.g., thaw of ground ice) but rather to primary wetland formation in areas where permafrost never aggraded. This interpretation aligns with the counterintuitive pattern where the warmer Horn Plateau shows limited thermokarst (**Figure 6e-f**), while the colder Arctic Red Plain exhibits extensive collapse features and ice-wedge polygons (**Figure 6E-F; Figure S9 in Supporting Information S1**). Rather than reflecting climate-driven permafrost degradation, these patterns suggest that the northernmost DPPs contain more ground ice susceptible to thaw, while southern DPPs likely never developed extensive or thick permafrost to begin with. Further, a large proportion of mapped DPPs are dominated by mature lichen communities (primarily *Cladonia* spp.), which require nearly a century to reach full development and are widely considered indicators of minimal disturbance [64]. The presence of recent thermokarst features within these undisturbed assemblages indicates that degradation can occur with the absence of wildfire, emphasizing internal hydrological and climate forcing. This contrasts with some sectors of the Bulmer Plain, where wider channelized fens and larger collapse scars occur despite no recent fire, and the cold Horn Plateau, where limited thermokarst are associated with fires [2]. These fundamental differences in landscape history, ground ice content, and permafrost thickness mean that northern and southern peatlands may not follow similar trajectories as warming continues.

Our findings also align with recent work on permafrost carbon dynamics in thawing peatlands. Harris et al. [65] documented significant carbon losses following permafrost thaw in boreal peatlands, with an average loss of ~33 g C m^{-2} $year^{-1}$ over 600 years. Given the extensive

673 distribution of DPPs across the Taiga Plains ecozone, their degradation represents a potentially
674 significant source of carbon to the atmosphere and DOC to fluvial networks. The landsystem
675 framework provides a basis for scaling site-specific carbon measurements to regional estimates
676 of current and future carbon release.

677 **6. Conclusions**

678 This research provides the first detailed description of dendritically-drained peat plateaus (DPPs)
679 as a distinctive permafrost landsystem in northwestern Canada. By applying a landsystem
680 approach, we have demonstrated how geological legacies conditioned by climate and ecological
681 factors have given rise to a characteristic assemblage of permafrost landforms with predictable
682 properties and vulnerabilities.

683 Dendritically-drained peat plateaus are composed of thick organic layers and developed
684 sequentially on gentle sloping till plains following deglaciation and the drainage of glacial Lake
685 Mackenzie. The oldest DPPs are dated to ~ 10,000 cal yr BP. Permafrost thickness beneath DPPs
686 reaches less than 20 m under peat plateaus, varying with proximity to water bodies and wetlands,
687 while taliks predominate beneath channelized fens and collapse scars, facilitating heat exchange
688 along frozen plateau margins.

689 Morphological patterns within DPPs exhibit substantial spatial variability that does not
690 follow a simple latitudinal gradient. DPP morphology is shaped by the extent of organic terrain,
691 which influences channelized fen configuration. Steeper slopes favor more compact, circular
692 basins, whereas gentle slopes promote large and elongated basins with linear drainage. Contrary
693 to expectations, the southernmost DPPs on the warmer Horn Plateau show relatively limited
694 degradation, characterized by low unfrozen wetland coverage, fewer channelized fens, and small
695 collapse scars. The Bulmer Plain, despite its similar latitude to the Horn Plateau, displays the most
696 advanced degradation, with extensive collapse scars and well-developed channelized fen
697 networks whereas the colder Arctic Red Plain ecoregion displays the second most degraded DPPs
698 areas. This variability indicates that local controls, including ground-ice content, elevation, air

699 temperature, precipitation, and drainage efficiency (slope) exert a stronger influence on DPP
700 shape than latitude alone.

701 The distribution of DPPs and their permafrost configuration reflects the interaction
702 between climate, hydrology, permafrost, and ecological feedback. Peatlands associated with
703 large fens and collapse bogs have thinner permafrost and are more sensitive to degradation than
704 previously thought, highlighting the vulnerability of these landforms to accelerated climate
705 warming. Understanding the controls, morphology, and distribution of DPPs provides valuable
706 insight into permafrost states in the northern Taiga Plains and offers a framework for monitoring
707 landscape change in a warming climate.

708
709

Acknowledgments

The authors would like to acknowledge the communities of Norman Wells, Tulit'a and Fort Good Hope in the Sahtu region, where this research takes place. We appreciate support from the Sahtu Secretariat Inc., Sahtu Renewable Resources Board (Tulit'a) and K'asho Got'ine Guardians during our work in the Sahtu region. We would like to thank Brielle Andersen, Joseph Young, Allison Rubin, and Alejandro Alvarez for their assistance on the field. We would also like to thank Alistair Monteath for assistance with the age-depth models. This research was supported by the Natural Sciences and Engineering Research Council of Canada (NSERC) through a Discovery Grant and Northern Research Supplement to DGF, and through the NSERC-funded PermafrostNet network. Fieldwork was supported by the Polar Continental Shelf Program, the Northern Scientific Training Program from Polar Knowledge Canada, the University of Alberta Northern Research Award, and the Northwest Territories Geological Survey. AC received scholarship support from the Fonds de recherche du Québec -- Nature et technologies, the Weston Family Foundation, and a 2022 Esri Canada GIS Scholarship

Author Contributions

Conceptualization: Alexandre Chiasson, Duane G. Froese, Steven V. Kokelj
Methodology: Alexandre Chiasson, Duane G. Froese, Steven V. Kokelj
Software: Alexandre Chiasson
Validation: Alexandre Chiasson, Duane G. Froese, Steven V. Kokelj
Formal Analysis: Alexandre Chiasson, Catherine La Farge-England
Investigation: Alexandre Chiasson, Duane G. Froese
Resources: Duane G. Froese, Steven V. Kokelj, Ashley Rudy,
Data Curation: Alexandre Chiasson, Jurjen Van der Sluijs
Writing - Original Draft: Alexandre Chiasson, Duane G. Froese, Steven V. Kokelj
Writing - Review and Editing: Alexandre Chiasson, Duane G. Froese, Steven V. Kokelj, Catherine La Farge-England, Ashley C.A. Rudy, Jurjen Van der Sluijs
Visualization: Alexandre Chiasson
Supervision: Duane G. Froese, Steven V. Kokelj
Project Administration: Duane G. Froese
Funding Acquisition: Duane G. Froese

References

1. Tarnocai, C., Kettles, I. M., & Lacelle, B. (2011). Peatlands of Canada (Geological Survey of Canada, Open File 6561).
2. Gibson, C., Cottenie, K., Gingras-Hill, T., Kokelj, S. V., Baltzer, J. L., Chasmer, L., & Turetsky, M. R. (2021). Mapping and understanding the vulnerability of northern peatlands to permafrost thaw at scales relevant to community adaptation planning. Environmental Research Letters, 16(5), 055022.
3. Smith, S. L., Romanovsky, V. E., Isaksen, K., Nyland, K. E., Shiklomanov, K. I., Streletskiy, D. A., and Christiansen, H. H. (2025). Permafrost [in "State of the Climate in 2024"]. Bulletin of the American Meteorological Society, 106(8): S338-S341.
4. O'Neill, H. B., Smith, S. L., Burn, C. R., Duchesne, C., & Zhang, Y. (2022). Widespread permafrost degradation and thaw subsidence in northwestern Canada. Journal of Geophysical Research: Earth Surface, 127(11), e2023JF007262.
5. Gibson, C. M., Chasmer, L. E., Thompson, D. K., Quinton, W. L., Flannigan, M. D., & Olefeldt, D. (2018). Wildfire as a major driver of recent permafrost thaw in boreal peatlands. Nature Communications, 9(1), 3041.
6. Quinton, W. L., Hayashi, M., & Pietroniro, A. (2003). Connectivity and storage functions of channel fens and flat bogs in northern basins. Hydrological Processes, 17(18), 3665–3684.
7. Hayashi, M., Quinton, W. L., Pietroniro, A., & Gibson, J. J. (2004). Hydrologic functions of wetlands in a discontinuous permafrost basin indicated by isotopic and chemical signatures. Journal of Hydrology, 296(1–4), 81–97.
8. Wright, N., Quinton, W. L., & Hayashi, M. (2008). Hillslope runoff from an ice-cored peat plateau in a discontinuous permafrost basin, Northwest Territories, Canada. Hydrological Processes, 22(15), 2816–2828.
9. Quinton, W. L., Hayashi, M., & Chasmer, L. E. (2011). Permafrost-thaw-induced land-cover change in the Canadian subarctic: Implications for water resources. Hydrological Processes, 25(1), 152–158.
10. Connon, R. F., Quinton, W. L., Craig, J. R., & Hayashi, M. (2014). Changing hydrologic connectivity due to permafrost thaw in the lower Liard River valley, NWT, Canada. Hydrological Processes, 28(14), 4163–4178.
11. Baltzer, J. L., Veness, T., Chasmer, L. E., Sniderhan, A. E., & Quinton, W. L. (2014). Forests on thawing permafrost: Fragmentation, edge effects, and net forest loss. Global Change Biology, 20(3), 824–834.
12. Haynes, K. M., Connon, R. F., & Quinton, W. L. (2018). Permafrost thaw induced drying of wetlands at Scotty Creek, NWT, Canada. Environmental Research Letters, 13(11), 114001.
13. Devoie, É. G., Craig, J. R., Dominico, M., Carpino, O., Connon, R. F., Rudy, A. C. A., & Quinton, W. L. (2021). Mechanisms of discontinuous permafrost thaw in peatlands. Journal of Geophysical Research: Earth Surface, 126, e2021JF006204.
14. Olefeldt, D., Persson, A., & Turetsky, M. R. (2014). Influence of the permafrost boundary on dissolved organic matter characteristics in rivers within the Boreal and Taiga plains of western Canada. Environmental Research Letters, 9(3), 035005.

15. Gordon, J., Quinton, W., Branfireun, B. A., & Olefeldt, D. (2016). Mercury and methylmercury biogeochemistry in a thawing permafrost wetland complex, Northwest Territories, Canada. Hydrological Processes, 30(20), 3627–3638.
16. Zoltai, S. C., & Tarnocai, C. (1975). Perennially frozen peatlands in the western Arctic and Subarctic of Canada. Canadian Journal of Earth Sciences, 12(1), 28–43.
17. Vitt, D. H., Halsey, L. A., & Zoltai, S. C. (1994). The bog landforms of continental western Canada in relation to climate and permafrost patterns. Arctic and Alpine Research, 26(1), 1–13.
18. Wishart, D., & Warburton, J. (2001). An assessment of blanket mire degradation and peatland gully development in the Cheviot Hills, Northumberland. Scottish Geographical Journal, 117(3), 185–206.
19. Pawson, R. R., Evans, M. G., & Allott, T. E. H. A. (2012). Fluvial carbon flux from headwater peatland streams: Significance of particulate carbon flux. Earth Surface Processes and Landforms, 37(11), 1203–1212.
20. Milner, A. M., Baird, A. J., Green, S. M., Swindles, G. T., Young, D. M., Sanderson, N. K., & Gałka, M. (2021). A regime shift from erosion to carbon accumulation in a temperate northern peatland. Journal of Ecology, 109(1), 125–138.
21. Evans, D., & Gooster, L. (2014). Glacial landsystems. Routledge.
22. Murton, J. B. (2021). What and where are periglacial landscapes? Permafrost and Periglacial Processes, 32(2), 186–212.
23. Kokelj, S. V., Wolfe, S. A., Weiss, N., Froese, D., Baltzer, J. L., Lantz, T., O'Neill, B. H., Morse, P. D., Sniderhan, A., Speetjens, N. J., van der Sluijs, J., Alvarez, A., Tank, S. E., & Gruber, S. (2026). Permafrost landsystems define variability in climate change effects on northern environments. Nature Communications.
24. Zernitz, E. R. (1932). Drainage patterns and their significance. The Journal of Geology, 40(6), 498–521.
25. Howard, A. D. (1967). Drainage analysis in geologic interpretation: A summation. AAPG Bulletin, 51(11), 2246–2259.
26. Glaser, P. H. (1987). The development of streamlined bog islands in the continental interior of North America. Arctic and Alpine Research, 19(4), 402–413.
27. Zoltai, S. C. (1988). Wetland environments and classification. In National Wetlands Working Group (Ed.), Wetlands of Canada (pp. 1–26). Polyscience Publications.
28. Szeics, J., MacDonald, G. M., & Oviatt, C. G. (1994). Holocene vegetation history of the central Mackenzie Mountains, Northwest Territories, Canada. Palaeogeography, Palaeoclimatology, Palaeoecology, 113(2–4), 347–358.
29. Ecosystem Classification Group. (2009). Ecological regions of the Northwest Territories – Taiga Plains. Department of Environment and Natural Resources, Government of the Northwest Territories.
30. Mackay, J. R., & Mathews, W. H. (1973). Geomorphology and Quaternary history of the Mackenzie River Valley near Fort Good Hope, N.W.T., Canada. Canadian Journal of Earth Sciences, 10(1), 26–41.
31. Smith, D. G. (1992). Glacial Lake Mackenzie, Mackenzie Valley, Northwest Territories, Canada. Canadian Journal of Earth Sciences, 29(8), 1756–1766.

32. Smith, D. G. (1994). Glacial Lake McConnell: Paleogeography, age, duration, and associated river deltas, Mackenzie River basin, western Canada. Quaternary Science Reviews, 13(9–10), 829–843.
33. Stoker, B. J., Margold, M., Gosse, J. C., Hidy, A. J., Monteath, A. J., Young, J. M., ... & Froese, D. (2022). The collapse of the Cordilleran–Laurentide ice saddle and early opening of the Mackenzie Valley, Northwest Territories, Canada, constrained by 10 Be exposure dating. The Cryosphere, 16(12), 4865–4886.
34. Couch, A. G., & Eyles, N. (2008). Sedimentary record of glacial Lake Mackenzie, Northwest Territories, Canada: Implications for Arctic freshwater forcing. Palaeogeography, Palaeoclimatology, Palaeoecology, 268(1–2), 26–38.
35. Stoker, B. J., Margold, M., Froese, D. G., Vickers, K. J., Cofaigh, C. Ó., Newton, M., Godbout, P. M., Menounos, B., Dunlop, P., & Dalton, A. S. (2024). Geomorphological record of Late Wisconsinan ice dynamics across western Northwest Territories, Canada. Geomorphology, 447, 109002.
36. Duk-Rodkin, A. (2002). Surficial geology, Norman Wells, Northwest Territories (Geological Survey of Canada, "A" Series Map 1989A, Scale 1:250,000). https://doi.org/10.4095/213617
37. Tarnocai, C., Canadell, J. G., Schuur, E. A. G., Kuhry, P., Mazhitova, G., & Zimov, S. (2009). Soil organic carbon pools in the northern circumpolar permafrost region. Global Biogeochemical Cycles, 23(2), GB2023.
38. Environment Canada. (2025). Canadian Climate Normals 1991-2020 Data. Norman Wells, Northwest Territories. Government of Canada. (accessed May 18, 2025).
39. Wright, S. N., Thompson, L. M., Olefeldt, D., Connon, R. F., Carpino, O. A., Beel, C. R., & Quinton, W. L. (2022). Thaw-induced impacts on land and water in discontinuous permafrost: A review of the Taiga Plains and Taiga Shield, northwestern Canada. Earth-Science Reviews, 232, 104104.
40. Heginbottom, J. A., Dubreuil, M. A., & Harker, P. A. (1995). Canada – Permafrost. In National Atlas of Canada (5th ed.). Natural Resources Canada, MCR 4177.
41. Duchesne, C., Chartrand, J., & Smith, S. L. (2020). Report on 2018 field activities and collection of ground-thermal and active-layer data in the Mackenzie corridor, Northwest Territories. Geological Survey of Canada Open File 8707.
42. Chiasson, A., Andersen, B., Alvarez, A., Moshtaghian, K., van der Sluijs, J., Rudy, A. C., Kokelj, S. V., & Froese, D. G. (2024a). Permafrost thickness variation on peat plateaus in the central Mackenzie Valley [Conference paper]. Proceedings of the 12th International Conference on Permafrost, Whitehorse, Yukon, Canada.
43. Kokelj, S. V., Gingras-Hill, T., Daly, S. V., Morse, P. D., Wolfe, S. A., Rudy, A. C. A., van der Sluijs, J., Weiss, N., O'Neill, H. B., Baltzer, J. L., Lantz, T. C., Gibson, C., Cazon, D., Fraser, R. H., Froese, D. G., Giff, G., Klengenberg, C., Lamoureux, S. F., Quinton, W. L., ... Young, J. M. (2023). The Northwest Territories Thermokarst Mapping Collective: A northern-driven mapping collaborative toward understanding the effects of permafrost thaw. Arctic Science, 9, 886–918.
44. Porter, C., Morin, P., Howat, I., Noh, M. J., Bates, B., Peterman, K., Keesey, S., Schlenk, M., Gardiner, J., Tomko, K., Willis, M., Kelleher, C., Cloutier, M., Husby, E., Foga, S., Nakamura, H., Platson, M., Wethington, M., Williamson, C., ... Bojesen, M. (2018). ArcticDEM [Data set]. Harvard Dataverse, V1. https://doi.org/10.7910/DVN/OHHUKH

45. Schumm, S. A. (1956). Evolution of drainage systems and slopes in badlands at Perth Amboy, New Jersey. Geological Society of America Bulletin, 67(5), 597–646.
46. Strahler, A. N. (1964). Quantitative geomorphology of drainage basin and channel networks. Handbook of Applied Hydrology.
47. Thornton, P. E., Shrestha, R., Thornton, M., Kao, S. C., Wei, Y., & Wilson, B. E. (2022). Gridded daily weather data for North America with comprehensive uncertainty quantification. Scientific Data, 9(1), 1–17.
48. 48. Pumple, J., Monteath, A., Harvey, J., Roustaei, M., Alvarez, A., Buchanan, C., & Froese, D. (2024). Non-destructive multi-sensor core logging allows for rapid imaging and estimation of frozen bulk density and volumetric ice content in permafrost cores. *The Cryosphere*, *18*(1), 489-503.
49. Lacelle, D., Fontaine, M., Forest, A. P., & Kokelj, S. (2014). High-resolution stable water isotopes as tracers of thaw unconformities in permafrost: A case study from western Arctic Canada. Chemical Geology, 368, 85–96.
50. Reimer, P. J., Austin, W. E. N., Bard, E., Bayliss, A., Blackwell, P. G., Bronk Ramsey, C., Butzin, M., Cheng, H., Edwards, R. L., Friedrich, M., Grootes, P. M., Guilderson, T. P., Hajdas, I., Heaton, T. J., Hogg, A. G., Hughen, K. A., Kromer, B., Manning, S. W., Muscheler, R., ... Talamo, S. (2020). The IntCal20 Northern Hemisphere radiocarbon age calibration curve (0–55 cal kBP). Radiocarbon, 62(4), 725–757.
51. Bronk Ramsey, C. (2009). Bayesian analysis of radiocarbon dates. Radiocarbon, 51(1), 337–360.
52. Kuhry, P., & Vitt, D. H. (1996). Fossil carbon/nitrogen ratios as a measure of peat decomposition. Ecology, 77(1), 271–275.
53. Loke, M. H., Acworth, I., & Dahlin, T. (2003). A comparison of smooth and blocky inversion methods in 2D electrical imaging surveys. Exploration Geophysics, 34(3), 182–187.
54. Herring, T., Lewkowicz, A. G., Hauck, C., Hilbich, C., Mollaret, C., Oldenborger, G. A., & Scandroglio, R. (2023). Best practices for using electrical resistivity tomography to investigate permafrost. Permafrost and Periglacial Processes, 34(4), 494–512.
55. Quinton, W. L., Hayashi, M., & Carey, S. K. (2008). Peat hydraulic conductivity in cold regions and its relation to pore size and geometry. Hydrological Processes, 22(15), 2829–2837.
56. Quinton, W. L., Hayashi, M., & Chasmer, L. E. (2009). Peatland hydrology of discontinuous permafrost in the Northwest Territories: overview and synthesis. Canadian Water Resources Journal, 34(4), 311–328.
57. Zoltai, S. C. (1993). Cyclic development of permafrost in the peatlands of northwestern Alberta, Canada. Arctic and Alpine Research, 25(3), 240–246.
58. Yi, S., Woo, M. K., & Arain, M. A. (2007). Impacts of peat and vegetation on permafrost degradation under climate warming. Geophysical Research Letters, 34, L16504.
59. Jones, B. M., Baughman, C. A., Romanovsky, V. E., Parsekian, A. D., Babcock, E. L., Stephani, E., Jones, M. C., Grosse, G., & Berg, E. E. (2016). Presence of rapidly degrading permafrost plateaus in south-central Alaska. The Cryosphere, 10, 2673–2692.
60. Mamet, S. D., Chun, K. P., Kershaw, G. G., Loranty, M. M., & Kershaw, G. P. (2017). Recent increases in permafrost thaw rates and areal loss of palsas in the Western Northwest Territories, Canada. Permafrost and Periglacial Processes, 28, 619–633.

61. Kurylyk, B. L., Hayashi, M., Quinton, W. L., McKenzie, J. M., & Voss, C. I. (2016). Influence of vertical and lateral heat transfer on permafrost thaw, peatland landscape transition, and groundwater flow. Water Resources Research, 52(2), 1286–1305.
62. Sjöberg, Y., Coon, E., Sannel, A. B. K., Pannetier, R., Harp, D., Frampton, A., Painter, S. L., & Lyon, S. W. (2016). Thermal effects of groundwater flow through subarctic fens: A case study based on field observations and numerical modeling. Water Resources Research, 52(3), 1591–1606.
63. Chiasson, A., van der Sluijs, J., Rudy, A. C. A., Kokelj, S. V., & Froese, D. G. (2024b). Permafrost degradation in dendritically-drained peat plateaus over the past 70 years in the central Mackenzie Valley [Conference paper]. Proceedings of the 12th International Conference on Permafrost, Whitehorse, Yukon, Canada.
64. Greuel, R. J., Degré-Timmons, G. É., Baltzer, J. L., Johnstone, J. F., McIntire, E. J., Day, N. J., ... & Cumming, S. G. (2021). Predicting patterns of terrestrial lichen biomass recovery following boreal wildfires. Ecosphere, 12(4), e03481.
65. Harris, L. I., Olefeldt, D., Pelletier, N., Blodau, C., Knorr, K. H., Talbot, J., & Turetsky, M. (2023). Permafrost thaw causes large carbon loss in boreal peatlands while changes to peat quality are limited. Global Change Biology, 29(19), 5720–5735.

Supporting Information

Dendritically-Drained Peat Plateaus: A Distinctive Thaw-Sensitive Organic-Rich Permafrost Landsystem in northwestern Canada

Chiasson, A[1,2,3]., La Farge-England, C.[4], Van der Sluijs, J[5]., Rudy, A.C.A[3]., Kokelj, S.V[3] & Froese, D.G[1,2]

1. Department of Earth and Atmospheric Sciences, University of Alberta, Edmonton, Canada.
2. Permafrost Archives Science Laboratory, Department of Earth and Atmospheric Sciences, University of Alberta, Edmonton, Canada.
3. NWT Geological Survey, Government of Northwest Territories, Yellowknife, Canada.
4. Department of Biological Sciences, University of Alberta, Edmonton, Alberta T6G 2E9, Canada.
5. NWT Centre for Geomatics, Government of Northwest Territories, Yellowknife, Canada

Correspondance:
Email: Alexandre_Chiasson@gov.nt.ca,
duane.froese@ualberta.ca

953
954
955 **Table S1.** 14C standard data. ^{14}C values were within expected ranges

Standard samples							
Core name	Sample Depth (CM)	Material	Sample ID	^{14}C age (yr BP)	±	Median age (cal. yr BP)	Calibrated 2s distribution (cal. yrBP range, %)
AVR-07-PAL-37 .18mgC	small mass sample	*Picea* fragment	UCIAMS-265219	43,360	180	45,717	Non-finite
AVR-07-PAL-37	-	*Picea* fragment	UCIAMS-265220	50,110	210	53,429	Non-finite age
FIRI-F	-	Wood fragment	UCIAMS-265221	4525	15	5150	5308-5265, 22.9%; 5242-5239, 0.4%; 5188-5052, 72.2%
IAEA-C5	-	Wood fragment	UCIAMS-265210	11,820	30	13,682	13,770-13,595, 94.8%; 13,536-13,531, 0.7%
IAEA-C5 .17mgC	-	Wood fragment	UCIAMS-265222	11,825	40	13,683	13,785-13,595, 94.4%; 13,536-13,530, 1%

956
957

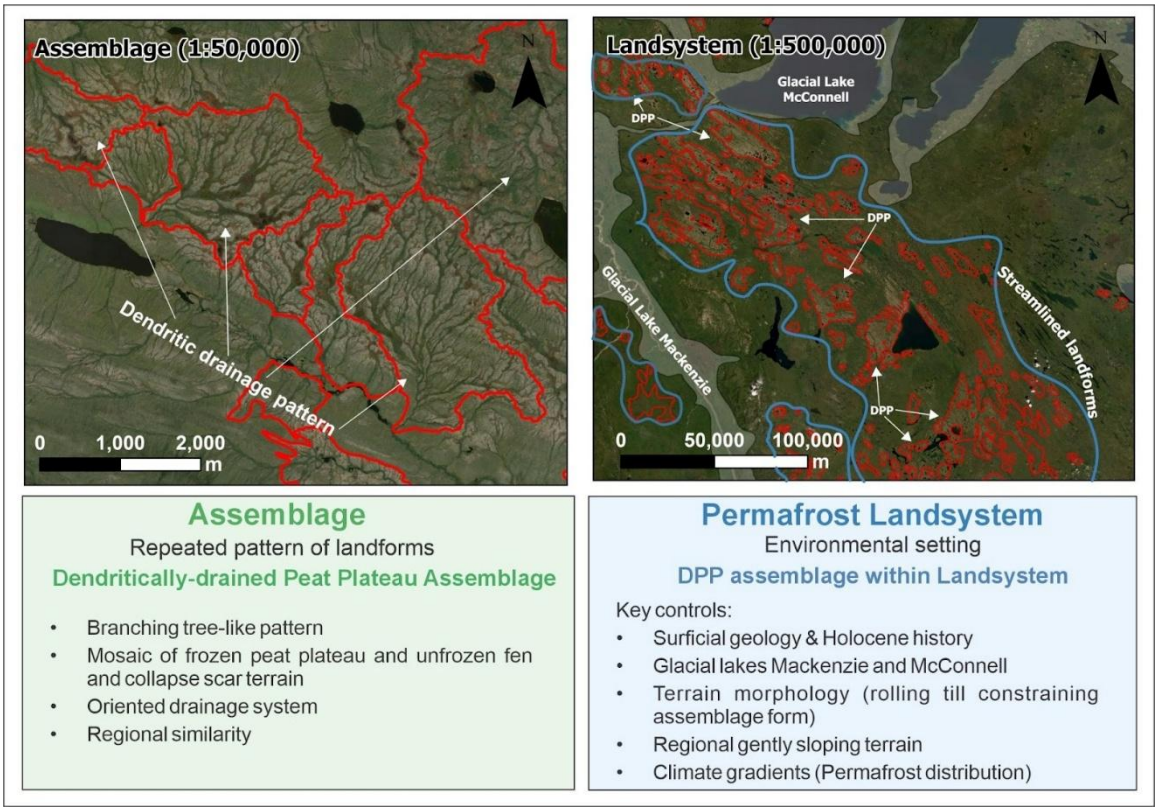

Figure S1. Conceptual framework between DPP landform assemblages and the broader permafrost landsystem. (Left) DPP assemblages at 1:50,000 scale showing the characteristic dendritic drainage pattern comprising a repeated mosaic of frozen peat plateaus, unfrozen fens, and collapse scar terrain. (Right) The permafrost landsystem at 1:500,000 scale showing multiple DPP assemblages (red polygons) within the broader environmental setting of the central Mackenzie Valley, including streamlined landforms and the extents of glacial lakes Mackenzie and McConnell (grey polygons).

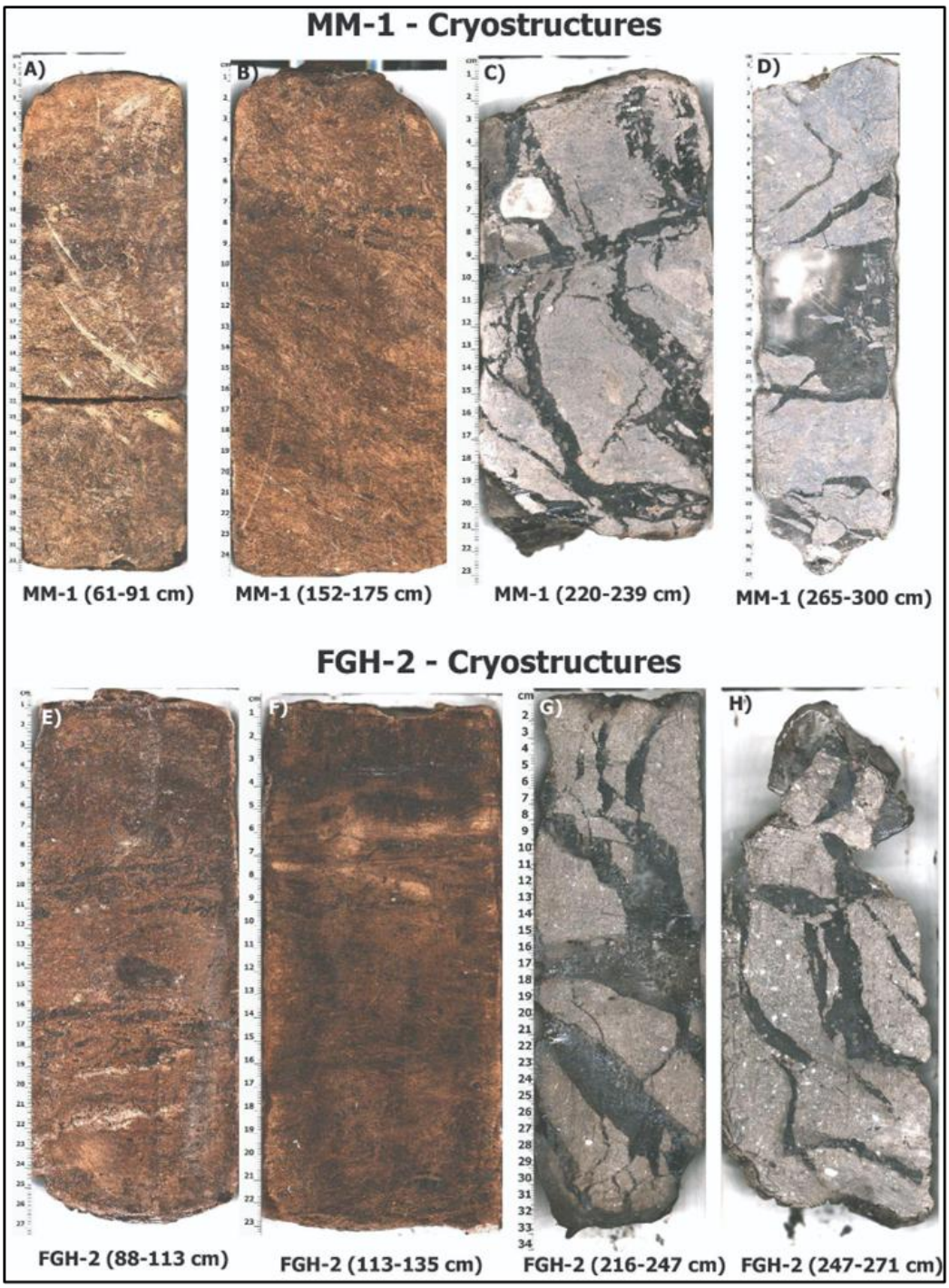

Figure S2. Permafrost cores collected at MM-01 and FGH-2. a) Structureless pore-ice peat; b) Structureless pore-ice peat; c) Crustal and lenticular cryostructures; d) Thick (~10 cm) ice lens within the diamict; e) Structureless ice-poor peat in FGH-2 core; f) Structureless ice-poor peat in FGH-2 core; g) Thick lenticular ice lenses, h) Thick lenticular ice lenses within coarse materials.

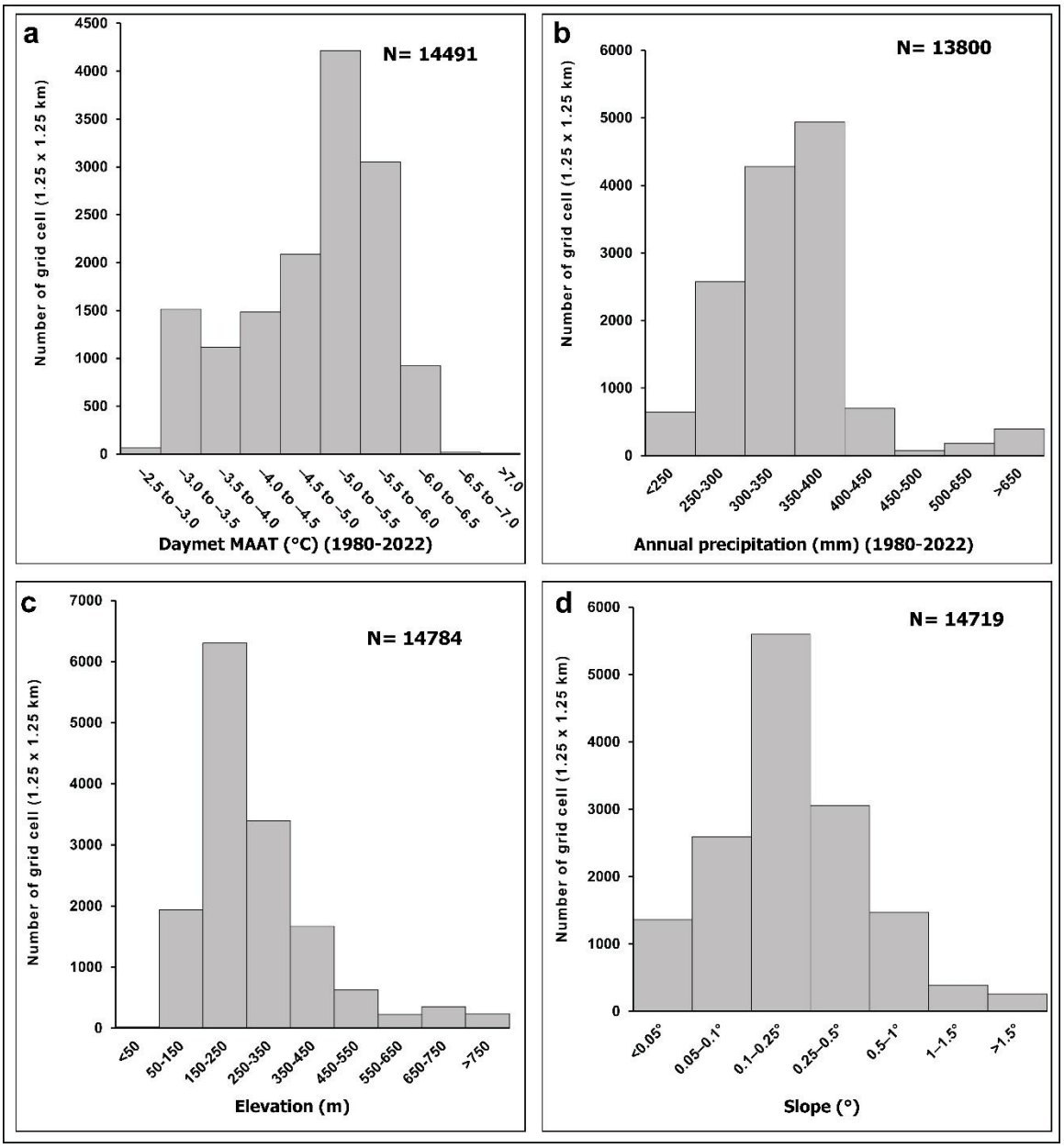

Figure S3. Histograms showing occurrence of DPPs within grid cells based on mean annual air temperature, annual precipitation, elevation, and slope.

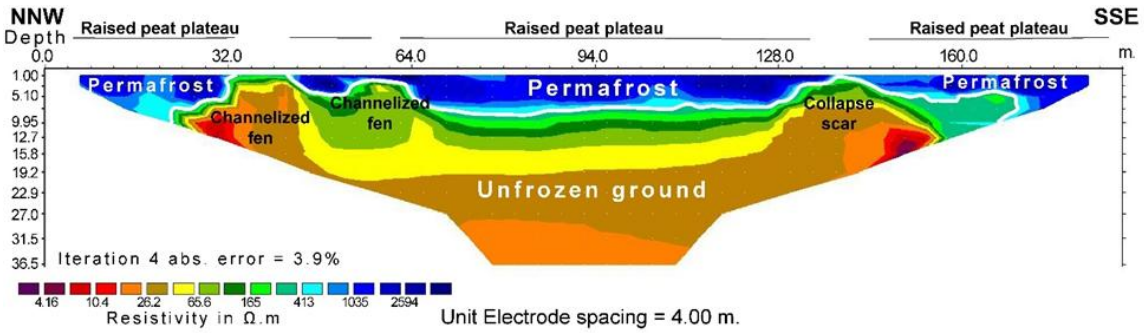

Figure S4. Electrical resistivity tomography surveys in June 2021 at MM-1 2 with inferred permafrost boundaries (white lines).

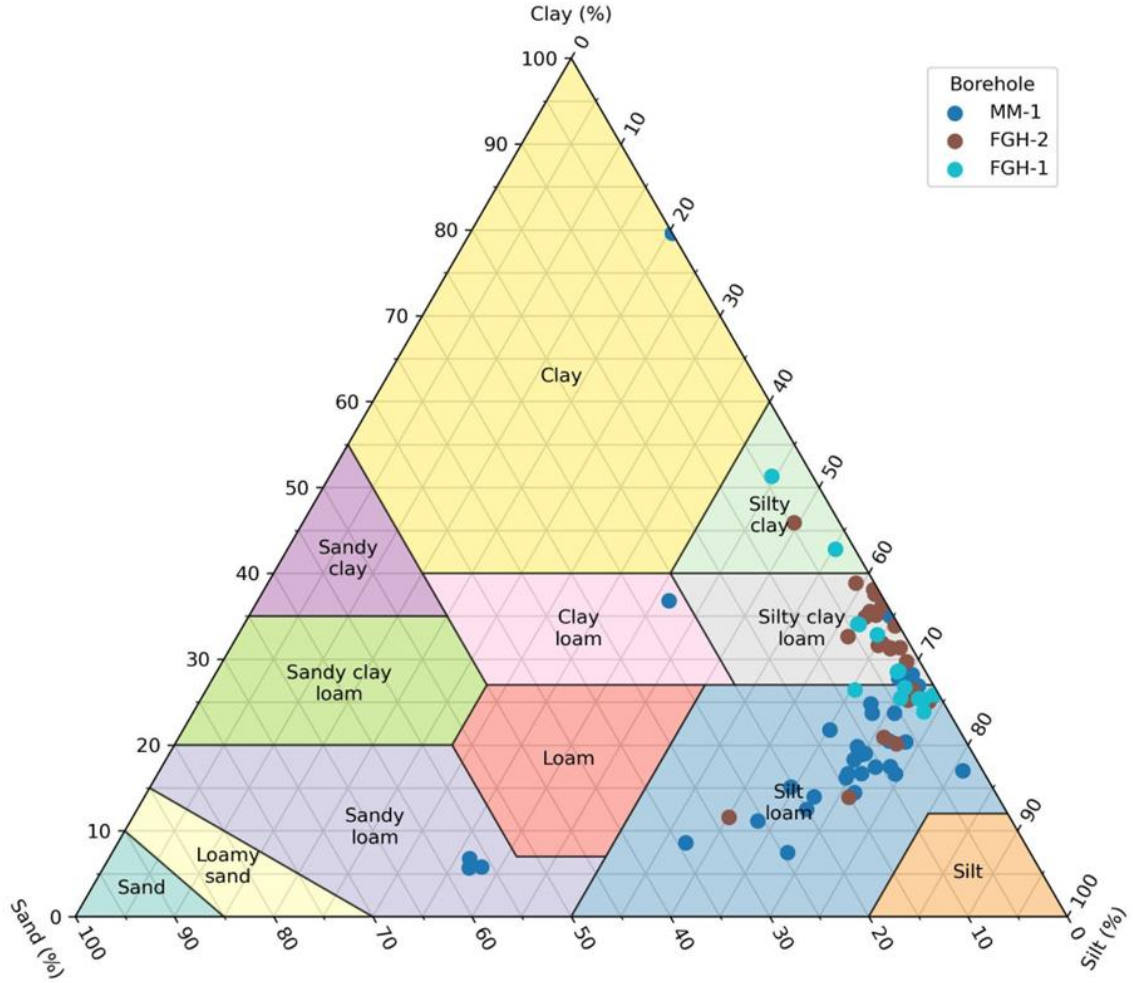

Figure S5. Borehole soil textures plotted over USDA soil texture classification.

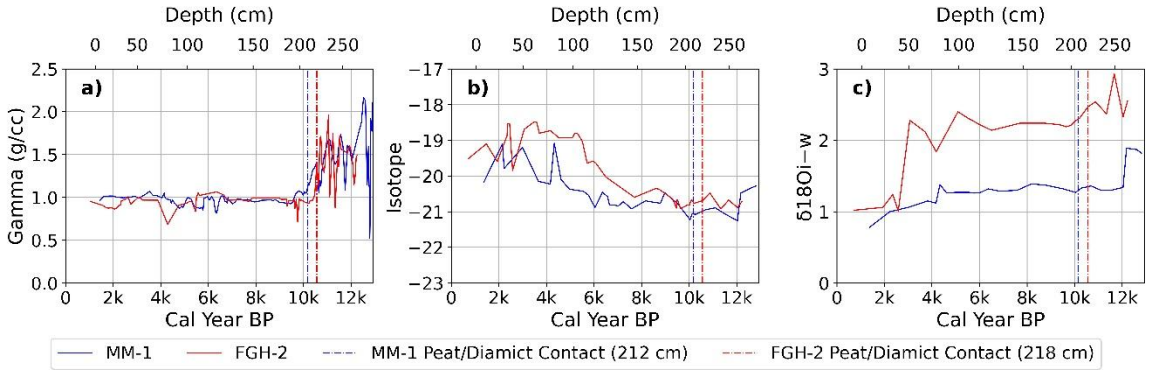

Figure S6. Stratigraphic and environmental parameter variations shown by radiocarbon (cal yr BP, ^{14}C) age-depth models for MM-1 and FGH-2, and by depth. Parameters include A) gamma density (g/cc), B) Isotope ($\delta^{18}O$ (‰)), and C) enrichment fraction ($\delta^{18}O_i$-w (‰). Red and blue lines represent environmental parameters from FGH-2 and MM-1, respectively. Dash-dot vertical lines indicate the peat/diamict stratigraphic contact for each core (MM-1: 212 cm; FGH-2: 218 cm).

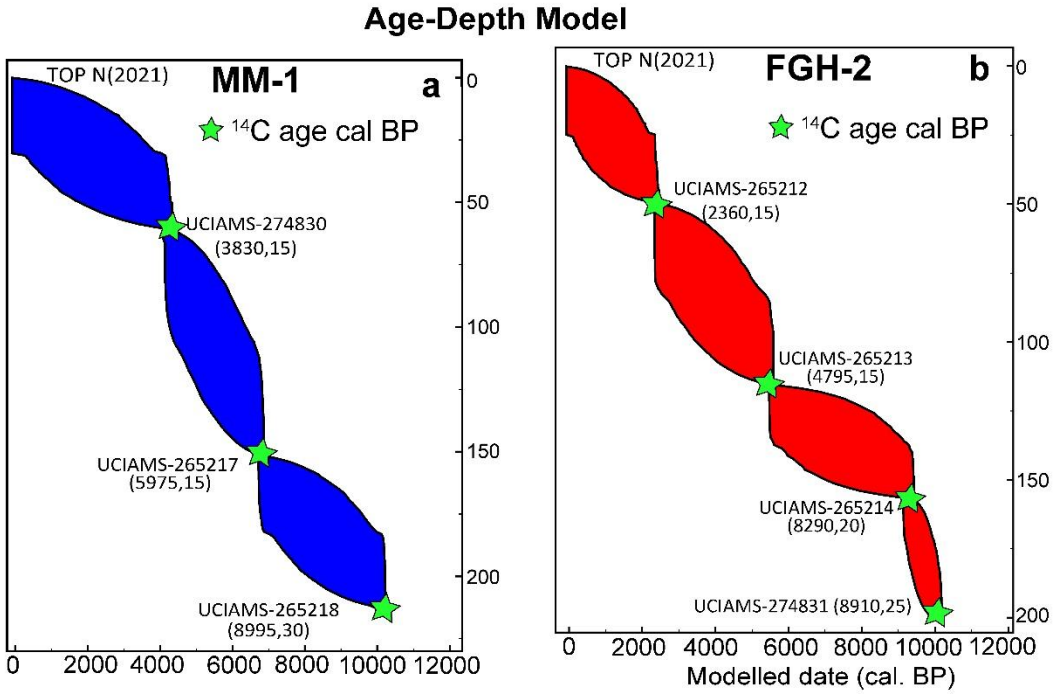

Figure S7. Bayesian age-depth model for A) MM-1 and B) FGH-2. Green stars indicate radiocarbon sample locations. UCIAMS laboratory codes are shown with calibrated radiocarbon ages (cal yr BP, ±1σ uncertainty). Blue (MM-1) and red (FGH-2) shaded areas show the 95% confidence intervals.

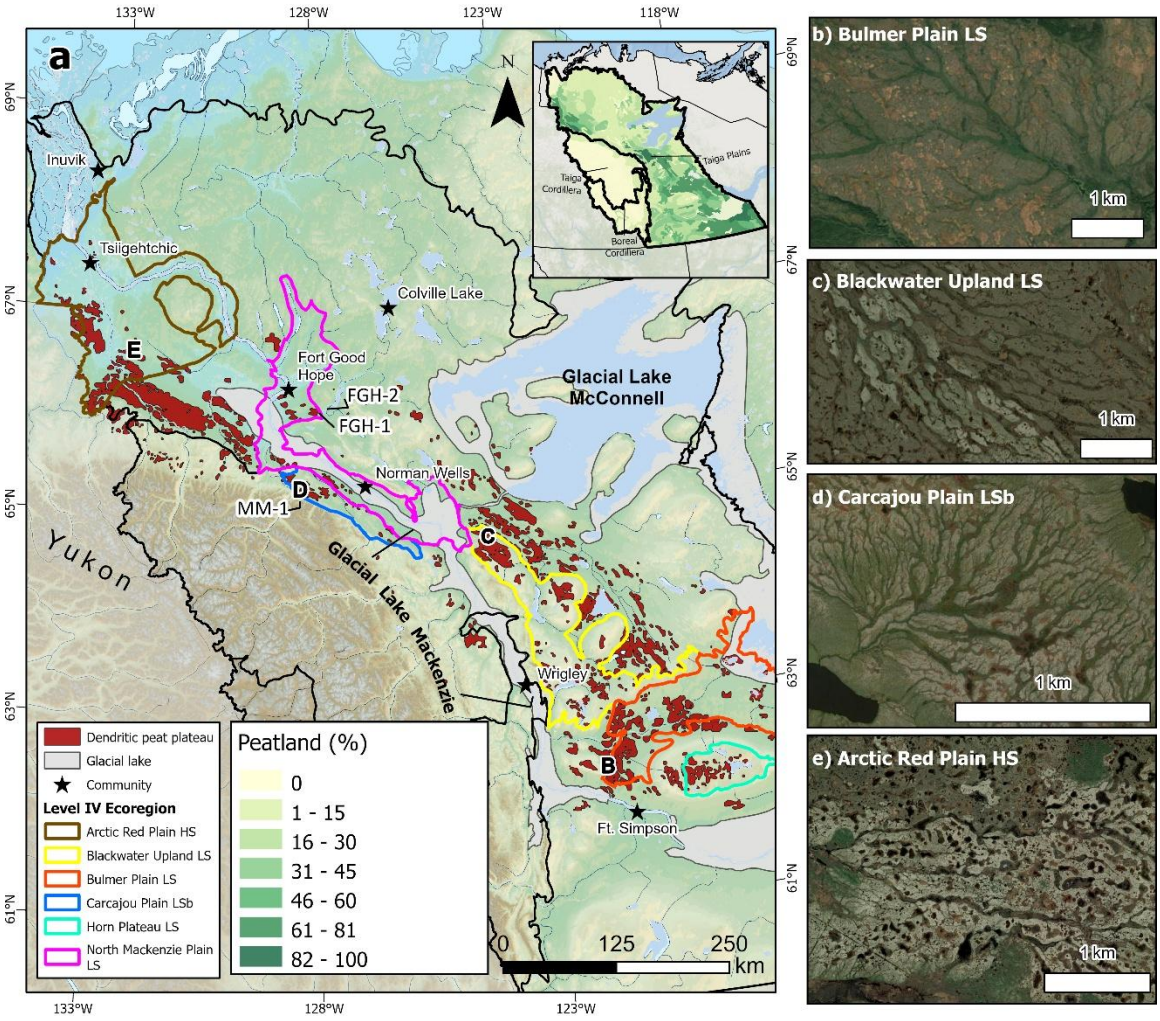

Figure S8. Distribution of DPPs (red) across the Taiga Plains ecozone with locations of DPP examples within Level IV Ecoregion from Figure 1. Maximum extent of glacial Lakes Mackenzie and McConnell from Smith (1992, 1994), and Couch and Eyles (2008). Peatland (%) layer modified from Tarnocai et al. (2011). Letters (B to E) refer to site locations shown in Figure 1. Base layer sources from GeoGratis.

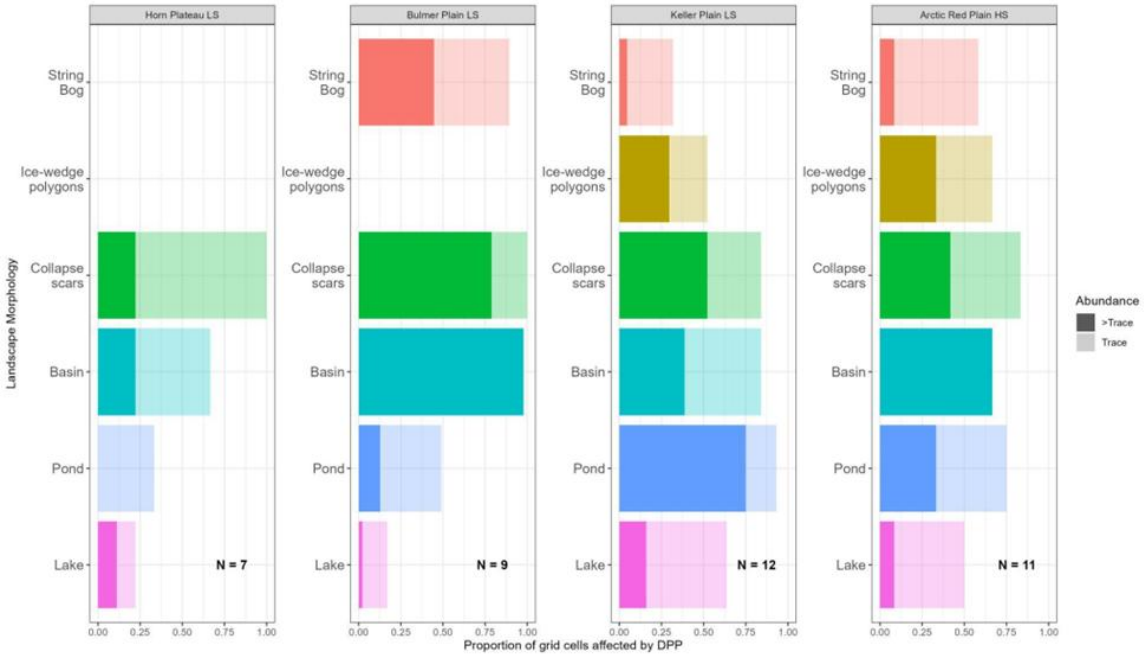

Figure S9. Proportion of grid cells with evidence of DPPs by landscape morphology in different Level IV ecoregions, showing percentage of grid cells with string bogs, periglacial features, and thaw physiography.

MM-1

Alexandre Chiasson - PhD project				
	Central Macknzie Valley Macrofossil IDs			**BFNA refernce for distribution data**
	samples washed in 42.5 um seive			
	flotation of subsample in distilled tap water			
	slides of distinct taxa as vouchers : parafilm enwrapped			
AC21-1-MM1-0				
Monolith	Lichen: Ascomyceta	Cladina stellaris (Opiz) Brodo	extant taxon	
0-20cm				
	Sphagnales: Sphagnaceae	**Sphagnum fuscum (Schimper) H. Klinggraff**	extant taxon	Capsules mature late summer. Mires, hummocks, fens; low to high elevations; Greenland; Alta., B.C., Man., N.B., Nfld. and Labr. (Nfld.), N.W.T., N.S., Nunavut, Ont., P.E.I., Que., Sask., Yukon; Alaska, Calif., Colo., Conn., Idaho., Ill., Ind., Maine, Md., Mass., Mich., Minn., Mont., N.H., N.J., N.Y., N.C., Ohio, Oreg., Pa., R.I., Utah, Vt., Va., Wash., W.Va., Wis., Wyo.; Eurasia.
		small br leaves; < 1 mm, stem leaves with; colour not dependable		Sphagnum fuscum is common in ombrotrophic mires and alpine mountain summits where it may form small to large hummocks to 1 m in height, more infrequently in weakly minerotrophic mires and richer fens.
		ringed pores on convex surface br leaves		
		stem no retort cells		
	Polytrichales: Polytrichaceae	Polytrichum commune Hedwig	extant taxon	Widely distributed in the North America, throughout temperate and boreal latitudes in the Northern Hemisphere, Mexico, Pacific Islands (New Zealand), Australia.
		marginal lamellae cell: groooved		
		toothed lf margins; long linear leaves		
	Dicranales: Dicranaceae	**Dicranum groenlandicum**	extant taxon	Capsules mature in summer. Arctic or alpine tundra, soil, humus or rocks, sometimes in bogs and fens; 10-3800 m; Greenland; Alta., B.C., Man., Nfld. and Labr. (Nfld.), N.W.T., Nunavut, Ont., Que., Yukon; Alaska, Colo., N.Y.; Europe; Asia.
		margins entire		
		upper marginal cells porose; basal str porose		
		alar cell region unistratose		
AC21-1-MM1-1				
30-33 cm	Whole sample Sphagnum 100%			
10-13 cm	**Sphagnales: Section Acutifolia**	**Sphagnum girgensohnii Russow**		Capsules mature late summer. Shade tolerant, forming carpets on moist forest floors, along small streams, up through subalpine zone; low to high elevations; Greenland; Alta. B.C., Man., N.B., Nfld. and Labr. (Nfld.), N.W.T., N.S., Nunavut, Ont., P.E.I., Que., Sask., Yukon; Alaska, Calif., Colo., Conn., Idaho., Ill., Ind., Maine, Md., Mass., Mich., Minn., N.H., N.J., N.Y., N.C., N. Dak., Ohio, Oreg., Pa., R.I., Tenn., Vt., Va., Wash., W.Va., Wis.; Eurasia.
		stem leaf and br leaf pore structure		
AC21-1-MM1-2	significantly degraded peat with some structure of plant material visible			
52-55 cm				
7-10 cm				
	woody stems and a cone woody "spinule?"			
	graminoids			
	rootlets			
	degraded leaf material from many different vascular plants			
	Bryophyte material: < 1% of sample			
	?	1 lf fragment with elongate porose basal cells (not identifiable)		
	Hypnales	1 complete leaf: cf Drepanocladus sp		
		lanceolate		
		elongate-linear laminal cell		
		margins distally serrulate		
		single costa to mid leaf or slightly more		
		cells smooth, basal cells sl porose		
		alars not distinct stem-leaf transition with isodiaametric cells		
	Hypnales	Drepanocladus cf aduncus		
		1 leaf (alar/basal most region missing):		
		ovate		
		single costa to mid leaf or slightly moe		
		elongate (sl porose) laminal cells thruought		
		margin (hint of a serrul along margin)		
AC21-1-MM1-3				
	Bryophyte material: 85%			
77-80 cm	Sphagnales	Sphagnum cf Section Cuspidatum		
		bulk of bryophyte material		
		chlorophyllous cells - more brdly on convex surface		
		no stem levs seen		
	Hypnales	Drepanocladus sensu lato	(cf Sarmentynum exannulatum /not D brevifolius st fal-sec) or cf Hematacaulis?	
		1 row of infl alars		
		ovate lanceolate		
		smooth leaves		
		elongate-linear cells		
		narrow lf base		
		acuminate		
		not fal-secund, more flexuose		
		margins denticulate (minutely)		
		stem x-section: no hyladermis		
		c strd: no different sm cells		
	Hypnales	single leaf fragment:		
		broad, sl concave, ovate base		
		elongate cells, nonporose		
		single costa		
		apex broken		
		costa x-section homogenous-thick walled		
		lamina unistratose		
AC21-1-MM1-6	5975 +/- 15	very fine material	scale of 1-5	
140-143		predominantly graminoid leaf fragment, rootlets		
	Sphagnales:Sphagnaceae	Sphagnum sp	**	
		1. slide w/lves & br		
		convex surface pore structure : Large pores at junct of cells		
		breakdown of fibrils		
		br with intact leaves		
		2. slide with Sphagnum detrital material; more degraded		

		unknown material?		
	Cyperaceae	Carex spp: 3 distinct spp - seeds	*	
		woody stems	*	
		rootlets	***	
		leaf fragments	****	
		faunal: bugs parts	*	
	Pinaceae:	Picea sp	*	
		spruce needles		
AC21-1-MM1-8	85% vplt/graminoid detrital material			
	Hypnales: Calliergonaceae:	**Calliergon richardsonii (Mitt.) Kindb. ex G. Roth.**	**	Wet, ± mineral-and nutrient-rich fens, ditches, shores, floating or submerged in lakes; low to high elevations; Greenland; Alta., Man., N.B., Nfld. and Labr., N.W.T., Nunavut, Ont., Que., Sask., Yukon; Alaska, Maine, Mich., Minn., Wyo.; n Eurasia; Pacific Islands (New Zealand).
178-181 cm		1/2-3/4 lgth costa, split		
3-6 cm		inflated alar cells		
		leaves in tact on stems, some frayed distally		
	Hypnales: Calliergonaceae:	**Pseudocalliergon turgescens (T. Jensen) Loeske**	+	Open, non-forested areas, lime-rich wetland habitats, small fens, small depressions in soil or on flat limestone rock, along rills or on rock flushed with calcium-rich water, submerged in small lakes or pools; low to high elevations; Greenland; Alta., B.C., Man., N.B., Nfld. and Labr., N.W.T., N.S., Nunavut, Ont., Que., Sask., Yukon; Alaska, Colo., Maine, Mass., Mich., Minn., Mont., N.Y., Ohio, Vt., Wyo.; South America (Bolivia, Peru); Eurasia; Africa.
		v small alar cells		
		no costa, sht double		
		linear laminal cells		
		orbicular erect spr d leaves		
	Hypnales: Calliergonaceae:	**Sarmentynum exannulatus (Wahlenb.) Tuom. & T.J. Kop.**	*	Intermediately mineral-rich fens, around springs, late snow beds, submerged in lakes; low to high elevations (0-4200 m); Greenland; Alta., B.C., Man., N.B., Nfld. and Labr., N.W.T., N.S., Nunavut, Ont., Que., Sask., Yukon; Alaska, Calif., Colo., Idaho, Maine, Md., Mass., Mich., Minn., Mont., Nev., N.H., N.Y., Oreg., Pa., Utah, Wash., Wyo.; Mexico; South America; Eurasia; Africa; Pacific Islands (New Zealand); Australia.
		costa 3/4 lf lngth		
		alar region: infl, margin to costa		
		serrulate lf margin		
	Cyperaceae	Cyperaceae seed w/ perigynium	+	
	Vplt	**Vasc plt leaf frag.: revolute margins elliptic leaves**	*	
	Vplt	beige rootlets v Plts	**	
	Graminoid	graminoid leaf fragments	***	
AC21-1-MM1-9		8995 +/- 30 BP; 211-214 cm		BFNA - distribution data
211-214		mineral soil particles	****	0.9
	Bryophytes	aquatic taxa: hydric site		
	Hypnales: Calliergonaceae	**Scorpidium cf scorpioides (Hedwig.) Lmpricht**	*	Fens, pools, lakeshores, submerged in lakes; low to high elevations (0-3600 m); Greenland; Alta., B.C., Man., N.B., Nfld. and Labr., N.W.T., N.S., Nunavut, Ont., Que., Yukon; Alaska, Colo., Conn., Ind., Maine, Mich., Minn., Mont., Utah, Vt., Wis., Wyo.; South America; Eurasia; Australia.
		linear-elongate laminal cells		
		lack of costa (ecostate phenotype)		
		strongly concave lvs		
		alar cells few		
		x-section of stem not possible (degraded)		
	Hypnales: Calliergonaceae	**Sarmentynum exannulatus (Wahlenb.) Tuom. & T.J. Kop.**	**	Intermediately mineral-rich fens, around springs, late snow beds, submerged in lakes; low to high elevations (0-4200 m); Greenland; Alta., B.C., Man., N.B., Nfld. and Labr., N.W.T., N.S., Nunavut, Ont., Que., Sask., Yukon; Alaska, Calif., Colo., Idaho, Maine, Md., Mass., Mich., Minn., Mont., Nev., N.H., N.Y., Oreg., Pa., Utah, Wash., Wyo.; Mexico; South America; Eurasia; Africa; Pacific Islands (New Zealand); Australia.
		Chiten-unknown arthropod		
		unknown material? Rnd capsule lids?		

FGH-2

FGH*PD1	Upper section			BFNA refernce for distribution data	
AC-21-1-FGH2	Lichen: Ascomyceta	Flavocetraria cucullata	extant taxon		
0-17 cm	Lichen: Ascomyceta	Cladina stygia	extant taxon		
monolith	**Sphagnales: Section Acutifolia**		extant taxon		Capsules mature late summer. Mires, hummocks, fens; low to high elevations; Greenland; Alta., B.C., Man., N.B., Nfld. and Labr. (Nfld.), N.W.T., N.S., Nunavut, Ont., P.E.I., Que., Sask., Yukon; Alaska, Calif., Colo., Conn., Idaho., Ill., Ind., Maine, Md., Mass., Mich., Minn., Mont., N.H., N.J., N.Y., N.C., Ohio, Oreg., Pa., R.I., Utah, Vt., Va., Wash., W.Va., Wis., Wyo.; Eurasia.
AC-21-1-FGH 2-1	**<2360 ± 15**				
(29-31)		Sphagnum Section Acutifolia:	intact stems with branches and leaves		
12-15cm			stem leaves resorbed at somewhat truncated apex; fibrils in stem lf cells bi-secting them; differentiated margin to apex region; broad lingulate leaves, long.; stem cells woth retort cels		
			br leaves: chlorocyst > exposed on concave surface; branch lf cell pores large filling space between fibrils, at distal tip of cellss and a few along commissures		
			colour not possible to determine		
	fine rootles				
	few woody, fine twigs/stems/br				
AC-21-1-FGH 2-2	**2360 +/- 15 yr BP**		few bryophytes		
52-55 cm					
12-15 cm				Notes	
	Sphagnales	Sphagnum Section Cuspidatum:	br leaves <1%	*	Sect Cuspidatum: chlorocyst > brdly exposoed on convex surface
	Rootlets		0.9	****	
	graminoid leaves		0.02	*	
	woody stem fragments		<1%	*	
	degraded lf material?		0.05	*	
	head casing of arthropod			+	
AC-21-1-FGH 2-5	**4795 +/- 15**		few bryophytes		
122-125 cm	woody twg fragments		<1%	*	
10-13 cm	spruce needles		+	*	
	vasc plt leaf fragments		0.05	*	
	graminoid lf fragments		0.85	***	
	Bryophyte lf fragments		<2%	*	
	Hypnales		costate 3/4 leaf		
			orbicular shape		
			linear lf cells		
			poss inf alars but not discernible		
			lves entire		
			obtuse apicies		
	Hypnales		non-costate		
			oblong		
			linear leaf cells		
			in terminal bud		
			obtuse apices		
			poss inf alars, but not discernible		
			many lf apices shreaded		
AC-21-1-FGH 2-6	**Hypnales**	**Pseudocalliergon turgescens (T. Jensen) Loeske**	linear lf cells, orbicular leaves, v sm alar & cells region; costa short double; sem x-sextion lacking distinct hyaline hyaldermis	*****	**Open, non-forested areas, lime-rich wetland habitats, small fens, small depressions in soil or on flat limestone rock, along rills or on rock flushed with calcium-rich water, submerged in small lakes or pools; low to high elevations; Greenland; Alta., B.C., Man., N.B., Nfld. and Labr., N.W.T., N.S., Nunavut, Ont., Que., Sask., Yukon; Alaska, Colo., Maine, Mass., Mich., Minn., Mont., N.Y., Ohio, Vt., Wyo.; South America (Bolivia, Peru); Eurasia; Africa.**
145-148 cm			intact leaves on stem but fragile to remove		
10-13 cm					
	gramminoid lf fragments			*	
	fine rootlets			*	
	blackened rootles			+	
AC-21-1-FGH 2-7	**Hypnales**	**Sarmetypnum cf exannulatus**	single costa	**	**(see below)**
170-173			inflated alar cells		
15-18 cm			margin serrulate		
			lanceolate lves		
			costa 3/4 lf lngth;		
	Section Acutifolium: Sphagnales	**Sphagnum sp**	leaves & some lve on branches		
			Large pore size		
	sm twigs				
	gramminoid lf fragments				
	vplt leaves		revolute margins, elliptic lf shpe		
	Cyperaceae seeds	5 pseeds with intact perigynia			
	black rootlets				
AC-21-1-FGH 2-8		rich deposit of bryophyte material 85%			
206-209 cm					
22-25 cm	**Hypnales: Calliergonaceae**	**Scorpidium scorpioides (Hedwig.) Lmpricht**	falcate, orbicular lves, sht costae visible	***	**Fens, pools, lakeshores, submerged in lakes; low to high elevations (0-3600 m); Greenland; Alta., B.C., Man., N.B., Nfld. and Labr., N.W.T., N.S., Nunavut, Ont., Que., Yukon; Alaska, Colo., Conn., Ind., Maine, Mich., Minn., Mont., Utah, Vt., Wis., Wyo.; South America; Eurasia; Australia.**
			sht laminal cells 70 µm		
			no alrs seen		
	Hypnales: Calliergonaceae	**Sarmetypnum exannulatus**		***	**Intermediately mineral-rich fens, around springs, late snow beds, submerged in lakes; low to high elevations (0-4200 m); Greenland; Alta., B.C., Man., N.B., Nfld. and Labr., N.W.T., N.S., Nunavut, Ont., Que., Sask., Yukon; Alaska, Calif., Colo., Idaho, Maine, Md., Mass., Mich., Minn., Mont., Nev., N.H., N.Y., Oreg., Pa., Utah, Wash., Wyo.; Mexico; South America; Eurasia; Africa; Pacific Islands (New Zealand); Australia.**
			costa > 1/2 lf, not into acumen		
			serrulate margin to base		
			well developed alar cells margin to costa		
			stem x-section not showing any hyalodermis		
			homogenous costa xsection (cells in xsect with circle protoplast region!)		
	Sphagnales	Sphagnum Section Acutifolia	leaves	*	
			Large pores		
			leaf x section: chlorocyts largest on concave surface of leaf		
	Cyperaceae	cf Carex sp	seeds w/ perigynia/ triangular	*	
	woody fragments		small twig frg	*	

	graminoids		rootlets, leaf fragments	*	